Desacetyl-α-melanocyte stimulating hormone and α-melanocyte stimulating hormone are required to regulate energy balance

Kathleen G Mountjoy[1,2,3,*], Alexandre Caron[4], Kristina Hubbard[1], Avik Shome[1], Angus C Grey[1,3,5], Bo Sun[1,3], Sarah Bould[1], Martin Middleditch[3,6], Beau Pontré[5], Ailsa McGregor[7], Paul W R Harris[3,6,8], Renata Kowalczyk[3,6,8], Margaret A Brimble[3,6,8], Rikus Botha[1,3], Karen M L Tan[9], Sarah J Piper[9], Christina Buchanan[2,3], Syann Lee[4], Anthony P Coll[9,10] and Joel K Elmquist[4]

[1]Department of Physiology, [2]Department of Molecular Medicine and Pathology, [3]Maurice Wilkins Centre for Molecular Biodiscovery, [5]Department of Anatomy and Medical Imaging, [6]School of Biological Sciences, [7]Department of Pharmacy, and [8]School of Chemical Sciences, University of Auckland, Private Bag 92019, Auckland 1142, New Zealand. [4]Department of Internal Medicine, Division of Hypothalamic Research, The University of Texas Southwestern Medical Center, Dallas, Texas, USA. [9]Department of Clinical Biochemistry, Cambridge Institute for Medical Research, Addenbrooke's Hospital, Cambridge CB2 2QR, United Kingdom and [10]University of Cambridge Metabolic Research Laboratories, MRC Metabolic Diseases Unit, Wellcome Trust-MRC Institute of Metabolic Science, Cambridge CB2 0QQ, UK

***Corresponding author.** K.G. Mountjoy, Department of Physiology, University of Auckland, 85 Park Road, Grafton 1142, Auckland, New Zealand. Email: kmountjoy@auckland.ac.nz. Ph: 64 9 373 7599 ext. 86447

ABSTRACT

Objective: Regulation of energy balance depends on pro-opiomelanocortin (POMC)-derived peptides and melanocortin-4 receptor (MC4R). Alpha-melanocyte stimulating hormone (α-MSH) is the predicted natural POMC-derived peptide that regulates energy balance. Desacetyl-α-MSH, the precursor for α-MSH, is present in brain and blood. Desacetyl-α-MSH is considered to be unimportant for regulating energy balance despite being more potent (compared with α-MSH) at activating the appetite-regulating MC4R *in vitro*. Thus, the physiological role for desacetyl-α-MSH is still unclear.

Methods: We created a novel mouse model to determine whether desacetyl-α-MSH plays a role in regulating energy balance. We engineered a knock in targeted QKQR mutation in the POMC protein cleavage site that blocks the production of both desacetyl-α-MSH and α-MSH from adrenocorticotropin ($ACTH_{1-39}$).

Results: The mutant $ACTH_{1-39}$ ($ACTH^{QKQR}$) functions similar to native $ACTH_{1-39}$ ($ACTH^{KKRR}$) at the melanocortin 2 receptor (MC2R) *in vivo* and MC4R *in vitro*. Male and female homozygous mutant $ACTH_{1-39}$ ($Pomc^{tm1/tm1}$) mice develop the characteristic melanocortin obesity phenotype. Replacement of either desacetyl-α-MSH or α-MSH over 14 days into $Pomc^{tm1/tm1}$ mouse brain significantly reverses excess body weight and fat mass gained compared to wild type (WT) ($Pomc^{wt/wt}$) mice. Here, we identify both desacetyl-α-MSH and α-MSH peptides as regulators of energy balance and highlight a previously unappreciated physiological role for desacetyl-α-MSH.

Conclusions: Based on these data we propose that there is potential to exploit the naturally occurring POMC-derived peptides to treat obesity but this relies on first understanding the specific function(s) for desacetyl-α-MSH and α-MSH.

Keywords: POMC, Obesity, Desacetyl-α-MSH, α-MSH, obese mouse model

1. INTRODUCTION

The melanocortin system plays a significant role in the regulation of energy balance (see reviews [1-3]). However, little is known about which specific endogenous pro-opiomelanocortin (POMC)-derived peptides are responsible for regulation of appetite, metabolism, and body weight. The POMC protein is inherently complex and is differentially cleaved into multiple peptides in a coordinated and tissue-specific manner [4]. POMC is a prohormone and its processing involves proteolytic cleavages at specific pairs of basic amino acids performed by enzymes, prohormone converting enzyme 1 (PC1), prohormone converting enzyme 2 (PC2) and carboxypeptidase E (CPE) (reviewed in [5]). In brain and pituitary pars distalis and pituitary pars intermedia, POMC is cleaved by PC1 to produce multiple peptides including $ACTH_{1-39}$ and β-lipotrophin (β-LPH). PC2 is selectively expressed in brain and pituitary pars intermedia and it cuts $ACTH_{1-39}$ further at tandem dibasic residues, KKRR, to produce $ACTH_{1-17}$ and corticotropin-like intermediate lobe peptide (CLIP). CPE subsequently removes basic amino acids at the C-terminus of $ACTH_{1-17}$ to produce $ACTH_{1-13}$. Post-translational processing of $ACTH_{1-13}$ produces desacetyl-α-MSH, α-MSH (monoacetylated) and diacetyl-α MSH. PC2 also cuts β-LPH to generate γ-LPH and β-endorphin.

One POMC-derivative, β-endorphin, stimulates food intake [6-8] while four POMC-derived peptides, $ACTH_{1-39}$, α-MSH, β-MSH and γ2-MSH reduce food intake [6, 9, 10]. A sixth peptide, desacetyl-α-MSH, also reduces food intake, but in pharmacological studies requires a 25-times higher dose than α-MSH [9]. For this reason, desacetyl-α-MSH has been considered to be unimportant for the regulation of energy balance [5, 11, 12]. However, there is a higher abundance of desacetyl-α-MSH compared with α-MSH in rat hypothalamus [13, 14]. In addition, desacetyl-α-MSH (compared with α-MSH) is more potent at activating the appetite-regulating MC4R *in vitro* [1]. Thus, the physiological role of desacetyl-α-MSH still remains unclear.

The melanocortin peptides differentially activate five melanocortin receptor (MCR) subtypes, each having unique tissue distributions and functions. MC3R and MC4R are highly expressed in the central nervous system and play key roles in regulating energy balance [15-17]. Multiple POMC-derived peptides activate MC3R and MC4R *in vitro* [18-20]. However, it is unknown whether these peptides have distinct or redundant roles *in vivo* [2]. Since studies have indicated that only pharmacologic concentrations of desacetyl-α-MSH (compared to α-MSH) inhibit food intake [9, 21], α-MSH is predicted to be the endogenous melanocortin peptide hormone that regulates energy balance. In addition, β-MSH is not present in rodents [22]. Here, we determined the direct contribution of desacetyl-α-MSH and α-MSH in regulating energy balance.

2. MATERIALS AND METHODS

2.1. Generation and maintenance of *Pomc*^{tm1} targeted mutation mouse model.

The objective of this study is to develop a mouse model with a targeted *Pomc* mutation that prevents production of desacetyl-α-MSH and α-MSH and then use this model to determine whether desacetyl-α-MSH plays a role in energy balance. Ozgene Pty Ltd (Bentley DC, WA, Australia) generated the *Pomc*^{tm1Kgm†} knock in mouse strain, the first targeted mutation (tm1) in the mouse *Pomc* gene that prevents ACTH$_{1\text{-}}$

† The registered nomenclature for this mouse model.

$_{39}$ cleavage into $ACTH_{1-17}$ and CLIP. We first validated that mutant $ACTH^{QKQR}$ (found in *Pomc*$^{tm1/tm1}$ mice) functions similar to wild type (WT) $ACTH^{KKRR}$ (found in *Pomc*$^{wt/wt}$ mice) both *in vitro* and *in vivo* (see Supplementary Data). A targeting vector was created containing mouse *Pomc* exon 3 KKRR proteolytic cleavage site mutated to QKQR with *PGK-Neo* selection cassette inserted downstream of WT exon 3. L*ox P* sites were inserted flanking WT exon 3 and the *PGK-Neo* selection cassette. The targeting vector was constructed from three fragments, the 5'homology arm, the 3'homology arm and the *lox P* arm, which were all generated by PCR. Cre-recombinase deletes the PGK-Neo cassette and WT exon 3 allowing the mutant QKQR exon 3 to be expressed. Following electroporation of the targeting construct into C57BL/6J Bruce4 embryonic stem (ES) cells, cells were selected for neomycin resistance. Southern blotting and PCR were used to confirm targeted ES cells. Euploid, targeted ES cells were then microinjected into *Balb/cJ* blastocysts and re-implanted into pseudo-pregnant dams. Resultant chimeras were bred to *C57BL/6J* breeders to establish transmission. Black progeny that were heterozygous for the gene-targeted allele were then bred to Cre recombinase "delete" mice on *C57BL/6J* background (Ozgene Pty Ltd) to allow excision of the WT exon 3 and Neo selection cassette. Cre was then removed by breeding to *C57BL/6J* WT mice. Resulting mice were transferred to the Vernon Jensen Animal Unit at the University of Auckland (UOA) where the colony is maintained with heterozygous breeding pairs. Mice were transferred from the University of Auckland to University of Texas South Western Medical Center (UTSW) where the colony is maintained with triplicate heterozygous mouse breeding.

Routine genotyping is performed by a PCR based strategy utilizing primers that anneal to *Pomc* exon 3 (forward 5'TGCATCCGGGCTTGCAAACTCGA3' and reverse 5’GGGGCAAGGAGGTTGAGAAAT3’) yielding an 820bp fragment. HaeII restriction enzyme is used to cleave the 802 bp fragment to yield 514bp, 234bp and 54 bp fragments. The QKQR mutation destroyed one of the HaeII sites and therefore HaeII cleaves the homozygous KI to yield 568bp and 234bp fragments.

2.2. Ethics and animal husbandry.

All experimental procedures involving mice at the Vernon Jensen Animal Facility, UOA, were approved by the Auckland University Animal Ethics Committee and conformed to The Animal Welfare Act 1999. Animals were housed up to 6 per cage on wood-chip bedding and maintained at room ambient 20°C with a 12-h dark-light cycle (lights on at 07:00 h in a pathogen-free barrier facility. The mice were fed regular chow (Teklad Global 18% protein rodent diet 2018 [Harlan Laboratories, Inc., Madison, WI, USA]). All experimental procedures for the metabolic cages were performed at UTSW and were approved by the IACUC committee at UTSW. The *Pomc*^{tm1Kgm} mouse breeding colony was established at UTSW to produce mice for testing in metabolic cages. At UTSW, mice were bred and housed in a barrier facility at room ambient 22-24°C on a 12 h light/12 h dark cycle and were provided standard chow (2016; Harlan Teklad) as well as water ad libitum. All experimental procedures involving mice at University of Cambridge were carried out in accordance with the guidelines of the United Kingdom Home Office. Animals were kept under controlled temperature (22°C) and 12 h light, 12 h dark schedule (lights on 7:00-19.00).

2.3. Growth and development.

Groups comprising *Pomc*$^{wt/wt}$, *Pomc*$^{wt/tm1}$ and *Pomc*$^{tm1/tm1}$ mice of each sex were weighed biweekly from weaning until 19-20 weeks of age. Significant differences were determined using two-way repeated-measures ANOVA and Bonferroni post-hoc test. Examination of both sexes allowed for assessment of sexually dimorphic phenotypes. At 27-30 weeks, the mice were fasted overnight before being euthanized with isoflurane, blood collected by cardiac puncture and nose-anus and anus-tail tip measurements recorded. Significant differences were determined using one-way ANOVA and Tukey's post-hoc test.

2.4. Body Composition.

Body composition was analyzed by magnetic resonance imaging (MRI) at the University of Auckland and nuclear magnetic resonance (NMR) at UTSW. MRI was used to assess body composition of *Pomc*$^{wt/wt}$, *Pomc*$^{wt/tm1}$ and *Pomc*$^{tm1/tm1}$ mice and to compare body composition of male *Pomc*$^{tm1/tm1}$ mice following melanocortin peptide treatment. NMR (minispec, Bruker) was used to compare body composition prior to metabolic cage experiments. MRI was performed using a 4.7T horizontal bore magnet interfaced with a UnityInova spectrometer (Agilent Technologies, Santa Clara, CA, USA). The anaesthetized animals were placed in a 72mm ID circularly-polarized radio-frequency coil for imaging (m2m Imaging, Cleveland, OH, USA). Localizer images were used to determine the appropriate position and number of slices to ensure that all of the animal's tissue was included in the body composition assessment. The scans to determine the body composition of the animals used the three-point Dixon technique [23] on a set of contiguous, 1mm thick slices with a field-of-view of 110 x 55 mm and the imaging matrix set to 256 x128. The repetition time (TR) was 1000 ms and the echo times were specified so that one in-phase image (0º) and two out-of-phase images (-180º, 180º) were acquired. All image processing to extract the fat and lean-tissue images from the MRI data and to determine the body composition was performed with MATLAB (Mathworks Inc., Natick, MA, USA) using previously described techniques [23]. Significant differences were determined using one-way ANOVA and Tukey's post-hoc test.

2.5. Metabolic Cages.

Metabolic measurements were obtained for male and female *Pomc*$^{wt/wt}$ and *Pomc*$^{tm1/tm1}$ mice aged ~ 4-6 weeks fed a regular chow diet or a regular chow diet and switched to a high-fat diet for the duration of the time they were housed in metabolic cages. Before each experiment body composition ad libitum fed mice was assessed using NMR spectrometer and the mice were acclimatized to individual caging for 3-4 days. Mice were then transferred to metabolic chambers for an additional 4-day acclimatization period with food provided ad libitum. Following acclimatization, energy expenditure (O_2 consumption) was measured by indirect calorimetry and simultaneous locomotor activity was assessed by infrared light-beam frame surrounding the cage using TSE Labmaster monitoring system (TSE Systems GmbH, Bad Homburg, Germany). Average oxygen consumption was calculated for both light and dark periods and expressed per total or lean body mass. For locomotor activity analysis, beam beaks in X- and Y- axis (ambulatory activity) was measured and summed over dark and light periods. Significant differences were determined using two-way repeated measures ANOVA and Bonferroni post-hoc analysis or unpaired two-tail Student's t test.

2.6. Central melanocortin peptide treatment.

We administered melanocortin peptides to mice continuously using osmotic mini pumps but first we determined using MALDI-TOF MS that α-MSH and desacetyl-α-

MSH dissolved in PBS and stored at 37°C were stable over 14 days. Aliquots of α-MSH and desacetyl-α-MSH dissolved in PBS that were prepared for treatment studies were incubated in Lo-bind eppendorf tubes at 37°C. At 7, 10 and 14 days aliquots were snap frozen at -80°C. After thawing, the aliquots were centrifuged at 13,000g for 2 min at 4 °C. Spots (1 μL) of each supernatant were then spiked on a MALDI-TOF plate and dried for ≥ 30 min in a vacuum dessicator. Matrix (αCyano-4-hydroxycinnamic acid in 50% acetonitrile in sterile water with 0.1% TFA) was applied manually over peptides and allowed to thoroughly dry before the plate was read in a Voyager DE-Pro Mass Spectrometer (Applied Biosystems). After dissolving in PBS, melanocortin peptides were primed overnight at 37 °C in osmotic mini pumps before being administered intracerebroventricular (i.c.v.) continuously over 14 days by osmotic mini pump infusions. Group-housed mice (n= 3-6 mice per cage) underwent stereotaxic surgery under isoflurane anesthesia to implant a cannula into the lateral cerebral ventricle with the following coordinates: anterior posterior 0.1 mm, medial lateral 0.9 mm with one spacer dorsal ventral. An Alzet® mini osmotic pump (Model 1002, Bio-Scientific Pty Ltd., NSW, Australia) filled either with saline vehicle (USP-IV-IM, Demo Pharmaceutical Industry, Greece) or melanocortin peptide (delivering 0.05 μg, 0.5 μg or 5 μg of peptide/ 25g mouse body weight/day) was implanted subcutaneously and was attached to the cannula using a catheter (Alzet Brain Infusion Kit 3, Bio-Scientific Pty Ltd.). Mice were allowed to recover from surgery for ~2-4 hour before being returned to their group-housed cages. Individual body weights and food and water intake for each cage were monitored daily over 14 days. All mice were monitored daily for signs of ill health (not eating, starry-fur, not moving). Significant differences were determined using two-way repeated measures ANOVA and Dunnett's post-hoc analysis.

2.7. Statistical analysis.

GraphPad Prism 7 software (GraphPad Software Inc., San Diego, CA) was used to perform all statistical analyses. Comparisons between groups were made by two-way or one-way repeated or non-repeated measures ANOVA with Tukey or Bonferroni post-hoc analysis, or by 2-tailed Student 't' test as indicated. Changes in body weight over time comparisons were made using repeated two-way ANOVA. $P<0.05$ was considered statistically significant. Data are presented as mean ± SEM.

3. RESULTS

3.1. A *Pomc* gene targeted mutation (*Pomc*^{tm1}) results in biologically active QKQR mutant ACTH$_{1\text{-}39}$ hormone.

Deletion in the *Pomc* gene results in obesity in both mice [24-26] and humans [27]. However, the *Pomc* null mouse is not suitable for determining specific POMC-derived peptide functions since it lacks all POMC-derived peptides and does not develop functional adrenal glands [24, 26, 28]. Thus, we developed a unique mouse model (*Pomc*^{tm1Kgm}) with a targeted QKQR mutation in the POMC protein cleavage site that is required to produce desacetyl-α-MSH and α-MSH from ACTH$_{1\text{-}39}$ (Figure 1A).

We performed a series of biochemical and physiological studies to validate biological activity for QKQR mutant ACTH$_{1\text{-}39}$ (ACTH^{QKQR}, see amino acid alignment, Figure 1B). ACTH^{QKQR} stimulates corticosterone production similar to native ACTH$_{1\text{-}39}$ (ACTH^{KKRR}) in dexamethasone-suppressed *Pomc*$^{wt/wt}$ male mice (Supplementary

Figure 1A). The $ACTH^{QKQR}$, like native $ACTH^{KKRR}$, is biologically active at the MC4R *in vitro* (Supplementary Figure 1B). *Pomc*$^{tm1/tm1}$ mice develop functional adrenal glands and produce corticosterone levels similar to *Pomc*$^{wt/wt}$ mice (Supplementary Figure 1C). These results confirm that $ACTH^{QKQR}$ is produced and functional in *Pomc*$^{tm1/tm1}$ mice.

3.2. $ACTH^{QKQR}$ protein is not cleaved to produce desacetyl-α-MSH and α-MSH.

We chose pituitary to validate that the QKQR mutation blocks $ACTH_{1\text{-}39}$ cleavage *in vivo* because POMC is abundantly expressed in pituitary pars distalis and pars intermedia while lesser amounts of POMC are expressed in the arcuate nucleus of the hypothalamus. The pituitary pars intermedia is a good surrogate for the arcuate nucleus since they both express PC2, the enzyme required for cleaving $ACTH_{1\text{-}39}$ to $ACTH_{1\text{-}17}$. The pars distalis and posterior lobe of the pituiatry are helpful controls since the pars distalis expresses POMC but no PC2 while the posterior lobe of the pituitary does not express either POMC or PC2.

To validate that $ACTH^{QKQR}$ protein is not cleaved, we used Matrix Assisted Laser Desorption/Ionization (MALDI)-Time-of-Flight (TOF) Mass Spectrometry (MS) of pituitary sections and lysates (see Supplementary Methods). MALDI-TOF MS imaging of pituitary sections confirms that diacetyl-α-MSH is present in *Pomc*$^{wt/wt}$ but not in *Pomc*$^{tm1/tm1}$ pars intermedia, while phospholipid (marker for pars distalis) [29] and vasopressin (marker for posterior pituitary lobe) [29] are present in the pars distalis and posterior lobe respectively, of both *Pomc*$^{wt/wt}$ and *Pomc*$^{tm1/tm1}$ mice (Figure 1C). In addition, a signal predicted to be Arg-CLIP (1-22; cleaved from the C-terminus of $ACTH_{1\text{-}39}$) is only detectable in *Pomc*$^{wt/wt}$ whole pituitary lysate

(Supplementary Figure 2A), while vasopressin, J peptide and a signal predicted to be β-LPH appear in both *Pomc*$^{wt/wt}$ and *Pomc*$^{tm1/tm1}$ whole pituitary lysate (Supplementary Figure 2A, B). $ACTH_{1\text{-}39}$ and β-LPH are the predominant POMC-derived peptides produced in pars distalis and diacetyl-α-MSH, α-MSH and β-LPH are the predominant POMC-derived peptides produced in pars intermedia. β-endorphin was not detected here but under conditions of stress, β-LPH in pars intermedia is cleaved by PC2 to produce β-endorphin [30]. Thus, in the *Pomc*$^{tm1/tm1}$ mouse only the $ACTH^{QKQR}$ is not cleaved *in vivo* to produce $ACTH_{1\text{-}13}$ and Arg-CLIP, while all other melanocortin peptides are produced through *in vivo* cleavage.

3.3. N-terminal acetylation of $ACTH^{QKQR}$ protein in whole pituitary lysate.

Surprisingly, MALDI-TOF MS showed a clear signal at m/z 4638 that appears only in *Pomc*$^{tm1/tm1}$ and not in *Pomc*$^{wt/wt}$ whole pituitary lysate (Supplementary Figure 2B). We identified this peptide as N-terminal acetylated $ACTH^{QKQR}$ using immunoprecipitation and LC-MS/MS. We determined that acetylation of $ACTH^{QKQR}$ does not change $ACTH^{QKQR}$ functional coupling at the mouse MC4R *in vitro* and it abolishes $ACTH^{QKQR}$ functional coupling of the mouse MC2R (Supplementary Figure 3A, B). Therefore, acetyl-$ACTH^{QKQR}$ produced in pituitary, presumably in pars intermedia where desacetyl-α-MSH is normally acetylated, is not expected to affect the phenotype of *Pomc*$^{tm1/tm1}$ mice.

3.4. Male and female *Pomc*$^{tm1/tm1}$ mice develop characteristic melanocortin obesity.

Despite expressing non-acetylated and acetylated $ACTH^{QKQR}$, which both functionally couple to the mouse MC4R *in vitro*, male and female *Pomc*$^{tm1/tm1}$ mouse body weights are significantly increased compared to *Pomc*$^{wt/wt}$ and *Pomc*$^{wt/tm1}$ mice starting at 4-6 weeks of age (Figure 1D, G), due to increased lean and fat mass. Female and male *Pomc*$^{tm1/tm1}$ body lengths are ~5% and ~3% longer respectively, compared to *Pomc*$^{wt/wt}$ or *Pomc*$^{wt/tm1}$ mice (Figure 1E, H). Quantitative magnetic resonance imaging (MRI) analysis of whole-body tissue composition at 26-29 weeks shows significant increases in fat mass in *Pomc*$^{tm1/tm1}$ male and *Pomc*$^{tm1/tm1}$ female mice compared with *Pomc*$^{wt/wt}$ mice (Figure 1F, I). These results indicate that the absence of desacetyl-α-MSH and α-MSH is sufficient to induce the characteristic melanocortin obesity phenotype, attributed to increased fat and lean mass as well as increased body length.

3.5. *Pomc*$^{tm1/tm1}$ mouse hyperphagia is exacerbated when mice are fed high-fat diet.

We next sought to determine what parameters of energy balance are altered and are causing obesity in early age. Mice (4 weeks of age) were individually housed in metabolic cages to investigate how the absence of desacetyl-α-MSH and α-MSH affects feeding behavior and energy expenditure, before differences in body weight might confound interpretation. While all *Pomc*$^{tm1/tm1}$ mice exhibit hyperphagia, we observed that male *Pomc*$^{tm1/tm1}$ mice fed a low-fat diet (LFD) have increased food intake during the light phase, while females are hyperphagic during the dark phase (Figure 2A, B). This suggests that male *Pomc*$^{tm1/tm1}$ mice have an altered feeding pattern, with abnormal food intake during the light-cycle. A deficiency in POMC or MC4R associates with hyperphagia that is exaggerated by dark-cycle food consumption (reviewed in [31, 32]) and is sensitive to dietary fat content [33, 34]. Here, we show high-fat diet (HFD) exacerbates hyperphagia in male and female

Pomc$^{tm1/tm1}$ mice throughout the day (Figure 2A, B), suggesting that the absence of desacetyl-α-MSH and α-MSH promotes food intake and potentially increases the palatability of HFD.

3.6. High-fat diet reduced energy expenditure for male and female *Pomc*$^{tm1/tm1}$ mice.

Manipulations of the melanocortin system were previously shown to impair energy expenditure, thus contributing to the obesity phenotype [34, 35]. Here, we observed that neither oxygen consumption nor locomotor activity was significantly altered in mice fed a LFD (Figure 2C - F). Interestingly, male and female *Pomc*$^{tm1/tm1}$ mice fed HFD exhibit significantly reduced oxygen consumption compared to *Pomc*$^{wt/wt}$ mice (Figure 2C, D), without changes in locomotor activity (Figure 2E, F). These data suggest that *Pomc*$^{tm1/tm1}$ mice have reduced energy expenditure when exposed to a HFD regimen.

3.7. Central administration of either desacetyl-α-MSH or α-MSH reverses *Pomc*$^{tm1/tm1}$ mouse obesity.

To determine whether replacement of each peptide alone can reverse the characteristic melanocortin obesity, we continuously administered incremental doses (0.03 -3.00 nmol / 25 g body weight / day) of α-MSH or desacetyl-α-MSH into adult *Pomc*$^{tm1/tm1}$ mouse brains over 14 days. First, we determined that α-MSH and desacetyl-α-MSH are stable under these treatment conditions (Supplementary Figure S4). We show that either α-MSH or desacetyl-α-MSH can significantly reduce body weight in *Pomc*$^{tm1/tm1}$ mice compared with vehicle-treated age- and sex-matched control *Pomc*$^{tm1/tm1}$ mice. Treatment with 5 μg α-MSH or 5 μg desacetyl-α-MSH similarly reduced male or female body weight (Figure 4E, F). However, α-MSH is more potent than desacetyl-α-MSH at reducing female body weight since body weight was significantly reduced following either 0.05 µg or 0.50 µg desacetyl-α-MSH but not by corresponding α-MSH doses (Figure 3A, B, F). In contrast with females, α-MSH is not more potent than desacetyl-α-MSH at decreasing male *Pomc*$^{tm1/tm1}$ mouse body weight and furthermore, there is a trend for desacetyl-α-MSH to be more potent than α-MSH (0.05 µg and 0.50 µg doses) at reducing male body weight (Figure 3C, D, F). The decreased body weight is predominantly due to fat mass loss: body weight and percent body fat measured using MRI in male *Pomc*$^{tm1/tm1}$ mice treated with either α-MSH or desacetyl-α-MSH are significantly reduced compared with vehicle-treated age-matched male *Pomc*$^{tm1/tm1}$ mice (Figure 4). The mice exhibited no signs of ill health over the 14 days of treatment and therefore these hormones do not appear to have any non-specific toxic effects.

4. DISCUSSION

The long-held myth that desacetyl-α-MSH is biologically unimportant for body weight regulation can now be put to rest. Our novel *Pomc*$^{tm1/tm1}$ mouse identifies desacetyl-α-MSH and α-MSH as both necessary for regulating mouse energy balance. We show that preventing the production of $ACTH_{1\text{-}13}$ from $ACTH_{1\text{-}39}$ results in a characteristic melanocortin obesity phenotype. Furthermore, pharmacological administration of desacetyl-α-MSH or α-MSH is sufficient to reverse this phenotype. Previously, central α-MSH administration has been shown to decrease rodent food intake and body weight [10, 36, 37], but we are the first to show potent effects for desacetyl-α-MSH decreasing mouse body weight. We show this because in our study, desacetyl-α-MSH is administered to a mouse that does not make any endogenous desacetyl-α-MSH or α-MSH. This leads to the question as to why central administration of desacetyl-α-MSH in *Pomc*$^{wt/wt}$ rodents does not decrease food intake similar to α-MSH [9]. We hypothesize that endogenous desacetyl-α-MSH and α-MSH prevent exogenously administered desacetyl-α-MSH from reducing food intake and body weight in *Pomc*$^{wt/wt}$ rodents. We propose that the balance between endogenous desacetyl-α-MSH and α-MSH levels dictates the regulation of mammalian energy homeostasis and furthermore we propose the balance of these peptides could be sexually dimorphic. Here we show sensitivity to desacetyl-α-MSH and α-MSH induced weight loss differs between the sexes; male mice exhibit similar sensitivity to desacetyl-α-MSH and α-MSH while female mice are more sensitive to α-MSH compared with desacetyl-α-MSH. This adds to a list of sexually dimorphic differences reported for POMC-derived peptide regulation of energy homeostasis [38-42].

Leptin has been shown to stimulate N-terminal acetylation of desacetyl-α-MSH to generate α-MSH in the rodent hypothalamus [12]. α-MSH is believed to be the biologically active melanocortin hormone mediating leptin inhibition of food intake because desacetyl-α-MSH, compared with α-MSH, was shown to rapidly degrade in the hypothalamus [12]. However, our study shows that desacetyl-α-MSH and α-MSH are similarly effective at reducing *Pomc*$^{tm1/tm1}$ mouse body weight when continuously infused at physiological levels into the lateral ventricle. Guo et. al. measured ~0.15 pmol α-MSH and ~0.58 pmol desacetyl-α-MSH in C57BL/6J mouse hypothalamus [12]. The lowest effective dose of either hormone that we infused i.c.v. into a 35g mouse is 0.029 pmol/minute and therefore if desacetyl-α-MSH is rapidly degraded *in vivo* it must trigger a rapid response prior to degradation. Importantly, we determined that both α-MSH and desacetyl-α-MSH are stable when stored in PBS at 37 °C for 14 days, which are the *in vivo* conditions for the osmotic mini pumps. Therefore, in our study the osmotic mini pumps should always be pumping intact hormones.

Our data also suggest for the first time that $ACTH_{1-39}$ is not sufficient to regulate mouse body weight despite $ACTH_{1-39}$ having full agonist activity at the MC4R (Supplementary Figure 3A) and the ability of exogenous $ACTH_{1-24}$ administered to rodent brain to cause decreased food intake [43]. However, it is unclear whether endogenous $ACTH_{1-39}$ is produced in the brain and if it is, it may not be expressed when and where MC4R are expressed. The major end-products of POMC processing detected in brain hypothalamus are desacetyl-α-MSH and β-endorphin [44, 45] while α-MSH and acetylated β-endorphin expression predominate in the brain stem [44]. Hence, *Pomc*$^{tm1/tm1}$ mouse brain is expected to express acetyl-ACTH^{QKQR} in brain stem and yet this is not sufficient to regulate *Pomc*$^{tm1/tm1}$ mouse body weight. The acetylation reaction required for producing α-MSH is documented to occur at desacetyl-α-MSH N-terminus [4, 44, 45]. However, here we show that N-terminal acetylation occurs on $ACTH_{1-39}$ when cleavage of $ACTH_{1-39}$ to $ACTH_{1-17}$ is prevented. Therefore in the *Pomc*$^{tm1/tm1}$ mouse, all cells and tissues that should normally express α-MSH are expected to express acetyl-ACTH^{QKQR}.

A disadvantage for our novel model is that the QKQR ACTH mutation is knocked in the mouse genome during embryogenesis and therefore it is possible that the absence of desacetyl-α-MSH and α-MSH during development contributes to the obese *Pomc*$^{tm1/tm1}$ mouse phenotype. Furthermore, our model has global removal of desacetyl-α-MSH and α-MSH and therefore we do not know whether the obese *Pomc*$^{tm1/tm1}$ mouse phenotype is due to the removal of these peptides in the brain, in the periphery, or in both brain and periphery. POMC is most abundantly expressed in the pituitary gland and expressed in lower abundance in the arcuate nucleus of the hypothalamus, the brainstem, and in several peripheral tissues including skin, pancreas, intestine, heart and reproductive organs [1]. However, our results do indicate that pituitary and adrenal gland development and function are unaltered in our model, as supported by normal histology and corticosterone levels respectively. This does not reflect the EC_{50} for $ACTH^{QKQR}$ that is 82-fold less than the EC_{50} for $ACTH^{KKRR}$ coupling to mMC2R (Supplementary Figure S3). We hypothesize that the negative feedback regulation of pituitary pars distalis $ACTH^{QKQR}$ production is significantly reduced resulting in a build-up of circulating $ACTH^{QKQR}$. $ACTH^{QKQR}$ is a full agonist (Supplementary Figure S3) at the mMC2R and this build-up of $ACTH^{QKQR}$ would account for the normal corticosterone levels in the *Pomc*$^{tm1/tm1}$ mouse. The development of a conditional *Pomc*$^{tm1/tm1}$ mouse model should resolve these issues.

For over 15 years we have understood that POMC-derived peptide hormones are required for regulation of food intake and energy expenditure but only now do we show that desacetyl-α-MSH and α-MSH are both key endogenous POMC-derived peptides responsible for mouse regulation of appetite, metabolism, and body weight. We hypothesize that physiological and environmental factors differentially regulate endogenous POMC-derived peptide processing leading to dynamic changes in abundance of each peptide produced in specific cell types in brain and pituitary, and these dynamic changes culminate in the regulation of appetite, metabolism and body weight. The recently discovered cannabinoid-induced ‘munchies’ mediated through POMC neurons in the brain, turning up the production of β-endorphin while turning down the production of α-MSH [46] supports this hypothesis. Our data could suggest that there is potential to exploit the naturally occurring POMC-derived peptides to treat obesity and type-2 diabetes but this relies on first understanding the specific function(s) for desacetyl-α-MSH and α-MSH in the brain and the periphery.

5. CONCLUSION

We show here that desacetyl-α-MSH is indeed biologically active *in vivo* and like α-MSH it can reduce mouse body weight and fat mass. Therefore, our study highlights a need to understand how endogenous desacetyl-α-MSH and α-MSH levels correlate with measures of energy balance and whether there are distinct or redundant roles for these POMC-derived peptides *in vivo*.

AUTHORS CONTRIBUTIONS

K.G.M. was responsible for the overall experimental design in Auckland, New Zealand. A.C., S.L. and J.K.E. were responsible for the experimental design and data analysis for the metabolic cage experiments at The University of Texas Southwestern Medical Center, USA. S.B., K.H., K. V B., A.S., and B.S. maintained the mouse colony at the University of Auckland, weighed mice, performed i.c.v. surgeries, euthanized mice, harvested tissues, analyzed data and contributed to writing of the manuscript. A.M. trained and supervised researchers performing i.c.v. surgeries. K.H. C.B. and M.M performed mass spectrometry on tissue and lysates and A.G. performed imaging mass spectrometry on pituitary. P.W.R.H., R.K. and M.A.B. synthesized native and mutant ACTH peptides. R.B. performed cell culture and adenylyl cyclase assays and analyzed this data. B.P. performed MRI and developed MRI data analysis. A.C., K.T., S.P. and K.H. performed testing of ACTH peptides *in vitro* and *in vivo*. K.G.M. with help from A.C., S.L and J.K.E. wrote the manuscript that was reviewed by all authors.

ACKNOWLEDGEMENTS

We thank J. Ross for help with MRI imaging analysis, K. Van Bysterveldt and M.Oudshoorn for help with mouse colony maintenance, harvesting tissues and preparing tissues for histology, K. Van Bysterveldt for help with cell culture and adenylyl cyclase assays, S. Amirapu and S. Cormack for help with histology and E. Thorstensen for steroid hormone assays. We received funding from the following New Zealand and University of Auckland funding bodies: The Marsden Fund, Auckland Medical Research Foundation, Maurice and Phyllis Paykel Trust, Maurice Wilkins Centre for Biodiscovery and Faculty Research and Development Fund. We also thank the Program Project Grant Core and Mouse Metabolic Phenotyping Core at The University of Texas Southwestern Medical Center at Dallas (supported by NIH grants PL1 DK081182 and UL1RR024923). This work was supported by NIH grant R37DK053301 to J.K.E. A.C is a Canadian Diabetes Association Post-doctoral Fellow. The work at Cambridge UK, was supported by Medical Research Council (MRC) (Award G108/617). A.P.C. was funded by the MRC Metabolic Disease Unit (MRC_MC_UU_12012/1). K.M.T. was supported by the Agency for Science Technology and Research (A*STAR) Singapore.

CONFLICTS OF INTEREST

The authors declare that no conflicts of interest exist.

APPENDIX. SUPPLEMENTARY DATA

Supplementary data includes methods and three supplementary figures.

REFERENCES

[1] Mountjoy, K.G., 2010. Functions for pro-opiomelanocortin- derived peptides in obesity and diabetes. Biochem. J. 428: 305-324.

[2] Coll, A.P., 2007. Effects of pro-opiomelanocortin (POMC) on food intake and body weight: mechanisms and therapeutic potential? Clin. Sci. 113: 171-182.

[3] Cone, R.D., 2006. Studies on the physiological functions of the melanocortin system. Endocr. Rev. 27: 736-749.

[4] Pritchard, L.E., White, A., 2007. Neuropeptide processing and its impact on melanocortin pathways. Endocrinology 148: 4201-4207.

[5] Pritchard, L.E., Turnbull, A.V., White, A., 2002. Pro-opiomelanocortin processing in the hypothalamus: impact on melanocortin signalling and obesity. J. Endocrinol. 172: 411-421.

[6] Tsujii, S., Bray, G.A., 1989. Acetylation alters the feeding response to MSH and beta-endorphin. Brain Res. Bull. 23: 165-169.

[7] Appleyard, S.M., Hayward, M., Young, J.I., Butler, A.A., Cone, R.D., Rubinstein, M., et al., 2003. A role for the endogenous opioid beta-endorphin in energy homeostasis. Endocrinology 144: 1753-1760.

[8] Low, M.J., Hayward, M.D., Appleyard, S.M., Rubinstein, M., 2003. State-dependent modulation of feeding behavior by proopiomelanocortin-derived beta-endorphin. Ann. N. Y. Acad. Sci. 994: 192-201.

[9] Abbott, C.R., Rossi, M., Kim, M., AlAhmed, S.H., Taylor, G.M., Ghatei, M.A., et al., 2000. Investigation of the melanocyte stimulating hormones on food intake. Lack Of evidence to support a role for the melanocortin-3-receptor. Brain Res. 869: 203-210.

[10] Millington, G.W., Tung, Y.C., Hewson, A.K., O'Rahilly, S., Dickson, S.L., 2001. Differential effects of alpha-, beta- and gamma(2)-melanocyte-stimulating hormones on hypothalamic neuronal activation and feeding in the fasted rat. Neuroscience 108: 437-445.

[11] Harrold, J.A., Williams, G., 2006. Melanocortin-4 receptors, beta-MSH and leptin: key elements in the satiety pathway. Peptides 27: 365-371.

[12] Guo, L., Munzberg, H., Stuart, R.C., Nillni, E.A., Bjorbaek, C., 2004. N-acetylation of hypothalamic alpha-melanocyte-stimulating hormone and regulation by leptin. Proc. Natl. Acad. Sci. U. S. A. 101: 11797-11802.

[13] Emeson, R.B., Eipper, B.A., 1986. Characterization of pro-ACTH/endorphin-derived peptides in rat hypothalamus. J. Neurosci. 6: 837-849.

[14] Frese, C.K., Boender, A.J., Mohammed, S., Heck, A.J., Adan, R.A., Altelaar, A.F., 2013. Profiling of diet-induced neuropeptide changes in rat brain by quantitative mass spectrometry. Anal. Chem. 85: 4594-4604.

[15] Huszar, D., Lynch, C.A., Fairchild-Huntress, V., Dunmore, J.H., Fang, Q., Berkemeier, L.R., et al., 1997. Targeted disruption of the melanocortin-4 receptor results in obesity in mice. Cell 88: 131-141.

[16] Chen, A.S., Marsh, D.J., Trumbauer, M.E., Frazier, E.G., Guan, X.M., Yu, H., et al., 2000. Inactivation of the mouse melanocortin-3 receptor results in increased fat mass and reduced lean body mass. Nat. Genet. 26: 97-102.

[17] Butler, A.A., Kesterson, R.A., Khong, K., Cullen, M.J., Pelleymounter, M.A., Dekoning, J., et al., 2000. A unique metabolic syndrome causes obesity in the melanocortin-3 receptor-deficient mouse. Endocrinology 141: 3518-3521.

[18] Roselli-Rehfuss, L., Mountjoy, K.G., Robbins, L.S., Mortrud, M.T., Low, M.J., Tatro, J.B., et al., 1993. Identification of a receptor for gamma melanotropin and

other proopiomelanocortin peptides in the hypothalamus and limbic system. Proc. Natl. Acad. Sci. U. S. A. 90: 8856-8860.

[19] Mountjoy, K.G., Mortrud, M.T., Low, M.J., Simerly, R.B., Cone, R.D., 1994. Localization of the melanocortin-4 receptor (MC4-R) in neuroendocrine and autonomic control circuits in the brain. Mol. Endocrinol. 8: 1298-1308.

[20] Mountjoy, K.G., Kong, P.L., Taylor, J.A., Willard, D.H., Wilkison, W.O., 2001. Melanocortin receptor-mediated mobilization of intracellular free calcium in HEK293 cells. Physiol. Genomics 5: 11-19.

[21] Mountjoy, K.G., Wu, C.S., Cornish, J., Callon, K.E., 2003. alpha-MSH and desacetyl-alpha-MSH signaling through melanocortin receptors. Ann. N. Y. Acad. Sci. 994: 58-65.

[22] Lee, Y.S., Challis, B.G., Thompson, D.A., Yeo, G.S., Keogh, J.M., Madonna, M.E., et al., 2006. A POMC variant implicates beta-melanocyte-stimulating hormone in the control of human energy balance. Cell Metab. 3: 135-140.

[23] Glover, G.H., 1991. Multipoint Dixon technique for water and fat proton and susceptibility imaging. J. Magn. Reson. Imaging 1: 521-530.

[24] Yaswen, L., Diehl, N., Brennan, M.B., Hochgeschwender, U., 1999. Obesity in the mouse model of pro-opiomelanocortin deficiency responds to peripheral melanocortin [see comments]. Nat. Med. 5: 1066-1070.

[25] Smart, J.L., Low, M.J., 2003. Lack of proopiomelanocortin peptides results in obesity and defective adrenal function but normal melanocyte pigmentation in the murine C57BL/6 genetic background. Ann. N. Y. Acad. Sci. 994: 202-210.

[26] Tung, Y.C., Piper, S.J., Yeung, D., O'Rahilly, S., Coll, A.P., 2006. A comparative study of the central effects of specific proopiomelancortin (POMC)-

derived melanocortin peptides on food intake and body weight in pomc null mice. Endocrinology 147: 5940-5947.

[27] Krude, H., Biebermann, H., Luck, W., Horn, R., Brabant, G., Gruters, A., 1998. Severe early-onset obesity, adrenal insufficiency and red hair pigmentation caused by POMC mutations in humans. Nat. Genet. 19: 155-157.

[28] Coll, A.P., Challis, B.G., Yeo, G.S., Snell, K., Piper, S.J., Halsall, D., et al., 2004. The effects of proopiomelanocortin deficiency on murine adrenal development and responsiveness to adrenocorticotropin. Endocrinology 145: 4721-4727.

[29] Larkin, S., Ansorge, O., Development and Microscopic Anatomy of the Pituitary Gland, in: L.J. De Groot, G. Chrousos, K. Dungan, K.R. Feingold, A. Grossman, J.M. Hershman, C. Koch, M. Korbonits, R. McLachlan, M. New, J. Purnell, R. Rebar, F. Singer, A. Vinik (Eds.), Endotext, South Dartmouth (MA), 2000.

[30] Madden, J.t., Akil, H., Patrick, R.L., Barchas, J.D., 1977. Stress-induced parallel changes in central opioid levels and pain responsiveness in the rat. Nature 265: 358-360.

[31] Garfield, A.S., Li, C., Madara, J.C., Shah, B.P., Webber, E., Steger, J.S., et al., 2015. A neural basis for melanocortin-4 receptor-regulated appetite. Nat. Neurosci. 18: 863-871.

[32] Krashes, M.J., Lowell, B.B., Garfield, A.S., 2016. Melanocortin-4 receptor-regulated energy homeostasis. Nat. Neurosci. 19: 206-219.

[33] Butler, A.A., 2006. The melanocortin system and energy balance. Peptides 27: 281-290.

[34] Butler, A.A., Marks, D.L., Fan, W., Kuhn, C.M., Bartolome, M., Cone, R.D., 2001. Melanocortin-4 receptor is required for acute homeostatic responses to increased dietary fat. Nat. Neurosci. 4: 605-611.

[35] Berglund, E.D., Liu, T., Kong, X., Sohn, J.W., Vong, L., Deng, Z., et al., 2014. Melanocortin 4 receptors in autonomic neurons regulate thermogenesis and glycemia. Nat. Neurosci. 17: 911-913.

[36] McMinn, J.E., Wilkinson, C.W., Havel, P.J., Woods, S.C., Schwartz, M.W., 2000. Effect of intracerebroventricular alpha-MSH on food intake, adiposity, c-Fos induction, and neuropeptide expression. American Journal of Physiology - Regulatory Integrative & Comparative Physiology 279: R695-703.

[37] Eerola, K., Nordlund, W., Virtanen, S., Dickens, A.M., Mattila, M., Ruohonen, S.T., et al., 2013. Lentivirus-mediated alpha-melanocyte-stimulating hormone overexpression in the hypothalamus decreases diet induced obesity in mice. J. Neuroendocrinol. 25: 1298-1307.

[38] Burke, L.K., Doslikova, B., D'Agostino, G., Greenwald-Yarnell, M., Georgescu, T., Chianese, R., et al., 2016. Sex difference in physical activity, energy expenditure and obesity driven by a subpopulation of hypothalamic POMC neurons. Mol Metab 5: 245-252.

[39] Bumaschny, V.F., Yamashita, M., Casas-Cordero, R., Otero-Corchon, V., de Souza, F.S., Rubinstein, M., et al., 2012. Obesity-programmed mice are rescued by early genetic intervention. J. Clin. Invest. 122: 4203-4212.

[40] Nohara, K., Zhang, Y., Waraich, R.S., Laque, A., Tiano, J.P., Tong, J., et al., 2011. Early-life exposure to testosterone programs the hypothalamic melanocortin system. Endocrinology 152: 1661-1669.

[41] Gelez, H., Poirier, S., Facchinetti, P., Allers, K.A., Wayman, C., Bernabe, J., et al., 2010. Neuroanatomical distribution of the melanocortin-4 receptors in male and female rodent brain. J. Chem. Neuroanat. 40: 310-324.

[42] Lippert, R.N., Ellacott, K.L., Cone, R.D., 2014. Gender-specific roles for the melanocortin-3 receptor in the regulation of the mesolimbic dopamine system in mice. Endocrinology 155: 1718-1727.

[43] Poggioli, R., Vergoni, A.V., Bertolini, A., 1986. ACTH-(1-24) and alpha-MSH antagonize feeding behavior stimulated by kappa opiate agonists. Peptides 7: 843-848.

[44] Eberle, A.N., 1988i The Melanotropins. Chemistry, Physiology and Mechanisms of action., S. Karger Publishers, Basel.

[45] Eberle, A.N., Proopiomelanocortin and the Melanocortin Peptides, in: R.D. Cone (Ed.), The Melanocortin Receptors, Humana Press Inc, Totowa, NJ, 2000, pp. 3-67.

[46] Koch, M., Varela, L., Kim, J.G., Kim, J.D., Hernandez-Nuno, F., Simonds, S.E., et al., 2015. Hypothalamic POMC neurons promote cannabinoid-induced feeding. Nature 519: 45-50.

FIGURE LEGENDS

Figure 1: Generation of *Pomc*$^{tm1/tm1}$ mice that develop the characteristic melanocortin obese phenotype.

A, Schematic of targeted *Pomc* allele for knock-in of QKQR mutation into *Pomc* exon 3 with resulting impact on pre-POMC processing and ACTH$_{1-13}$ production.
B, Amino acid sequence alignments for native and mutant ACTH$_{1-39}$ molecule.
C, MALDI imaging MS shows ACTH$_{1-13}$ is successfully deleted from *Pomc*$^{tm1/tm1}$ mouse pituitary. Mass-to-charge (m/z) signals that delineate the pars distalis (PD, m/z

835 in *blue* represents phospholipid) and posterior lobe (P, m/z 1086 in *red* represents vasopressin) are shown. In addition, diacetyl-α-MSH (m/z 1706 in *green*) is detected in the pars intermedia (PI) of *Pomc*$^{wt/wt}$ but not *Pomc*$^{tm1/tm1}$ tissue. Scale bars = 500 μM.

D and G, Body weights of mice fed a regular-chow diet from weaning. Significant difference determined using two-way repeated-measures ANOVA and Bonferroni post-hoc test between *Pomc*$^{wt/wt}$ and *Pomc*$^{tm1/tm1}$. *, $p< 0.05$; **, $p<0.01$; ***, $p < 0.001$ or using paired Student 't' test between *Pomc*$^{wt/wt}$ and *Pomc*$^{tm1/tm1}$; male $^{\#}$, $p<0.05$; female $^{\#\#}$, $p<0.01$

E and H, Body length measured at 27-30 weeks for mice fed a regular-chow diet from weaning. Data are shown as mean ± SEM. Significant differences determined using one-way ANOVA and Tukey's post-hoc test. *, $p< 0.05$; **, $p<0.01$

F and I, Percent body fat calculated from 6 MRI Dixon images/mouse. Data are shown as mean ± SEM for mice aged 26-29 weeks and fed a regular-chow diet. Significant differences determined using one-way ANOVA and Tukey's post-hoc test. ***, $p<0.001$; ****, $p<0.0001$

Figure 2: **Food intake and energy expenditure for male and female *Pomc*$^{wt/wt}$ and *Pomc*$^{tm1/tm1}$ mice.**

A and B, Food intake was automatically measured in metabolic cages for mice at 4 weeks of age and fed regular chow for 4 days and then switched to high-fat diet for 4 days (n = 5-6 mice/group). Mice were acclimatized to the metabolic cages for 5 days prior to experiments. Data are shown as average food intake ± SEM per light cycle over 4 consecutive days for males and females. Significant differences determined using either two-way repeated measures ANOVA and Bonferroni post-hoc analysis or unpaired two-tail Student's t test. *, $p<0.05$; ***, $p<0.001$

C and D, Oxygen consumption (VO_2) measured in metabolic cages for the same mice shown in A and B. Data shown as average VO_2 per light cycle ± SEM over 4 consecutive days for males and females. Significant differences determined using either two-way repeated measures ANOVA and Bonferroni post-hoc analysis or unpaired two-tail Student's t test. *, $p<0.05$; **, $p<0.01$

E and F, Locomotor activity measured in metabolic cages for same mice as shown in A and B. Data are shown as total activity per light cycle ± SEM over 4 consecutive days for males and females. No significant differences were determined using either two-way repeated measures ANOVA and Bonferroni post-hoc analysis or unpaired two-tail Student's t test.

Figure 3: Central α-MSH or desacetyl-α-MSH treatments reduce male and female *Pomc*$^{tm1/tm1}$ mouse body weight.

A, B, C, D, E, F Administration (i.c.v.) of α-MSH or desacetyl-α-MSH compared to vehicle treatment reduced *Pomc*$^{tm1/tm1}$ mouse body weight. At the start of treatment male mice were aged 23-31 weeks and female mice were aged 29-31 weeks. Vehicle or peptide dose (µg/25g mouse body weight on day1/day) was continuously administered over 14 days. Combined data are shown as mean ± SEM for two independent experiments. A- D; Significant differences determined using two-way repeated measures ANOVA and Dunnett's post-hoc analysis. E, F: Significant differences determined using two-way ANOVA and Dunnett's post-hoc analysis. *, $p<0.05$; **, $p<0.01$; ***, $p<0.001$.

Figure 4: Central α-MSH or desacetyl-α-MSH treatment reduces male *Pomc*$^{tm1/tm1}$ mouse fat mass.

A and C, Mean body weight ± SEM for male *Pomc*$^{tm1/tm1}$ mice (n = 3 group) after 14 days i.c.v administration of vehicle, α-MSH or desacetyl-α-MSH.

B and D, Percent body fat ± SEM determined by MRI for male *Pomc*$^{tm1/tm1}$ mice shown in A and C after 14 days i.c.v administration of vehicle, α-MSH or desacetyl-α-MSH. Significant differences between vehicle and peptide treatment determined using unpaired, two-tailed Student's t test. *, $p<0.05$; **, $p<0.01$; ***, $p<0.001$

E, Representative MRI images for mice presented in A, - D. Fat and lean tissues represented as green and red, respectively.

SUPPLEMENTARY DATA

MATERIALS and METHODS

1. Materials.

Diacetyl-α-MSH, α-MSH, desacetyl-α-MSH, β-MSH and $ACTH_{1-24}$ were purchased from Bachem AG (Bubendorf, Switzerland). Native $ACTH_{1-39}$, QKQR mutant $ACTH_{1-39}$, KGGR mutant $ACTH_{1-39}$, KQRQ mutant $ACTH_{1-39}$ and acetyl-QKQR mutant $ACTH_{1-39}$ were purchased from Pepscan (Zuiderstuisweg 2, The Netherlands) or synthesized in-house. A rabbit polyclonal antibody (KM4) that specifically recognizes α-MSH and desacetyl-α-MSH, but not $ACTH_{1-24}$, $ACTH_{1-39}$, γ-MSH or β-MSH, was made in-house. *O*-(6-Chlorobenzotriazol-1-yl)-*N*,*N*,*N′*,*N′*-tetramethyluronium hexafluorophosphate (HCTU), and Fmoc-amino acids were purchased from GL Biochem (Shanghai, China). Fmoc-amino acids were supplied with the following side-chain protection: Fmoc-Asn(Trt)-OH, Fmoc-Arg(Pbf)-OH, Fmoc-Glu(O*t*Bu)-OH, Fmoc-Gln(Trt)-OH, Fmoc-His(Trt)-OH, Fmoc-Lys(Boc)-OH, Fmoc-Ser(*t*Bu)-OH, Fmoc-Trp(Boc)-OH, Fmoc-Tyr(*t*Bu)-OH. Fmoc-Phe-$OCH_2PhOCH_2CH_2CO_2H$ (Fmoc-Phe-HMPP) was purchased from PolyPeptide Group (Strasbourg, France). *N*,*N*-Diisopropylethylamine (*i*Pr_2NEt), piperidine, acetic anhydride (Ac_2O), ***N*,*N′*-diisopropylcarbodiimide (DIC), 3,6-dioxa-1,8-octane-dithiol (DODT), formic acid,** 1-methyl-2-pyrrolidinone (NMP) **and t**riisopropylsilane (*i*Pr_3SiH) were purchased from Sigma-Aldrich (St. Louis, Missouri). *N,N*-Dimethylformamide (DMF) and acetonitrile (MeCN) were supplied from Scharlau (Barcelona, Spain). Dichloromethane (CH_2Cl_2) was purchased from ECP Limited (Auckland, New Zealand). Trifluoroacetic acid (TFA) was purchased from Halocarbon (River Edge, New Jersey). Aminomethyl polystyrene resin was synthesized following literature procedures [1, 2].

2. Synthesis, purification and analysis of "KKRR" native $ACTH_{1\text{-}39}$, "QKQR" mutant $ACTH_{1\text{-}39}$ and acetyl-"QKQR" mutant $ACTH_{1\text{-}39}$.

Aminomethyl polystyrene resin (0.1 mmol) was swollen in CH_2Cl_2 (5 mL, 30 min), drained and then reacted with Fmoc-Phe-HMPP (2.0 equiv), and DIC (2.0 equiv) in CH_2Cl_2 (2.0 mL) for 2 h at room temperature. Subsequent steps of Fmoc SPPS were performed using the Fmoc/*t*Bu strategy and Liberty 12 Microwave Peptide Synthesizer (CEM Corporation, Mathews, NC). All amino acid couplings were performed as single coupling cycles, with the exception of Fmoc-Arg(Pbf)-OH and Fmoc-His(Trt)-OH where a double coupling cycle was performed as part of a synthetic protocol recommended by CEM Microwave Technology. Protected amino acids were incorporated using Fmoc-AA-OH (5.0 equiv, 0.2 M), HCTU (4.5 equiv, 0.45 M), and $i Pr_2NEt$ (10 equiv, 2 M) in DMF, for 5 min, at 25 W and maximum temperature of 75 ºC, except Fmoc-Arg(Pbf)-OH and Fmoc-His(Trt)-OH. Fmoc-Arg(Pbf)-OH was initially coupled for 25 min at room temperature which was followed by the second coupling for 5 min, at 25 W and maximum temperature of 72 ºC. Fmoc-His(Trt)-OH was initially coupled for 10 min at room temperature which was followed by the second coupling for 5 min, at 25 W and maximum temperature of 50 ºC The Fmoc group was removed using 20% piperidine in DMF (30 s followed by a second deprotection for 3 min at 62 W and maximum temperature of 75 ºC). For the synthesis of the acetyl-"QKQR" Mutant $ACTH_{1\text{-}39}$ the final *N*-acetylation of the free N^{α}-amino group of *N*-terminal serine was performed using 20% Ac_2O in NMP (2 x). Resin cleavage and removal of the amino acid side-chain protecting groups was undertaken by incubating the resin in TFA/*i*Pr_3SiH/H_2O/DODT (v/v/v/v; 94/1/2.5/2.5) cleavage cocktail for 2 h at room temperature. The crude peptides were precipitated and triturated with cold diethyl ether, isolated (centrifugation), dissolved in 50% MeCN (aq) containing 0.1% TFA and lyophilized.

Analytical reverse phase high-performance liquid chromatography (RP-HPLC) was performed using a Dionex P680 using Waters XTerra® analytical column (MS C_{18}, 150 mm x 4.6 mm; 5 μm), at a flow rate of 1 mL/min, and using the 5%B to 65%B over 20 min, *ca*. 3%B per min gradient system. The solvent system used was A (0.1% TFA in H_2O) and B (0.1% TFA in MeCN) with detection at 210 nm, 254 nm, and 280 nm. The ratio of products was determined by integration of spectra recorded at 210 nm.

A Hewlett Packard (Palo Alto, CA) 1100MSD mass spectrometer was used for ESI-MS analysis in the positive mode. Peptides were purified using a Waters 600E system using Waters XTerra® semi-preparative column (C_{18}, 300 mm x 19 mm; 10 μm), at a flow rate of 10 mL/min, and using the 5%B to 20%B over 15 min, *ca*. 1%B per min, and then 20%B to 75%B over 550 min, *ca*. 0.1%B per min gradient system. Fractions were collected, analyzed by either RP-HPLC or ESI-MS, pooled and lyophilized, to give the "KKRR" Native $ACTH_{1-39}$ (11.8 mg, 98% purity); R_t 13.30 min; *m/z* (ESI-MS) 917.1 ($[M + 5H]^{5+}$ requires 917.4), "QKQR" Mutant $ACTH_{1-39}$ (6.0 mg, 99% purity); R_t 13.41 min; *m/z* (ESI-MS) 911.5 ($[M + 5H]^{5+}$ requires 911.8), and acetyl-"QKQR" Mutant $ACTH_{1-39}$ (19.2 mg, 98% purity); R_t 13.70 min; *m/z* (ESI-MS) 920.0 ($[M + 5H]^{5+}$ requires 920.8), as white amorphous solids.

3. Testing mutations in $ACTH_{1-39}$ for effects on $ACTH_{1-39}$ functional activity.

3.1. *In Vivo*: Dexamethasone-suppression test.

Adult male *Pomc*$^{wt/wt}$ mice were acclimatized to handing for 1 week before the start of the experiment. At 0900 hour on the day of experiment each mouse received 0.4 mg (100 µL) dexamethasone sodium phosphate by intraperitoneal (ip) injection. After 2 h, the mice received via subcutaneous injection 100 µL vehicle (0.5% bovine serum albumin [BSA] in phosphate buffered saline [PBS]), $ACTH_{1-39}$ (1 µg) or mutant $ACTH_{1-39}$ peptide (1 µg). One hour later, the mice were euthanized by cervical dislocation, blood collected by cardiac puncture and plasma prepared for steroid hormone measurement.

3.2. *In Vitro*: Cre-luciferase activity.

HEK293 cells were transfected with human MC4R, cAMP responsive luciferase construct (LUC) and internal control plasmid, pRL-CMV (Promega Corp., Madison, Wisconsin, USA) which constitutively expresses *Renilla* luciferase. After transfection, cells were serum starved for 8 h before increasing doses of peptide were added and the cells incubated for 16 h at 37°C. The cells were then lysed and luciferase reporter activity analyzed as previously described [3].

4. MALDI-TOF MS to identify POMC-derived peptides expressed in pituitary cryosections and pituitary lysates.

Sections (10 µM) of snap-frozen *Pomc*$^{wt/wt}$ and *Pomc*$^{tm1/tm1}$ adult mouse pituitaries were sectioned at -21°C on a cryostat and mounted onto either a glass slide for H&E staining or a MALDI-TOF plate ready for Mass Spectrometry (MS). The adjacent sections on the glass slide were used to determine which sections on the MALDI-TOF plate included the pars intermedia of the pituitary. Spots (1 µL) of 10 µM purified peptide stocks (diacetyl-α-MSH, α-MSH, desacetyl-α-MSH and $ACTH_{1-24}$) were also spiked on the MALDI-TOF plate to get near-point calibration data for molecular weight determination. The MALDI-TOF plates with sections and peptides were dried for ≥30 min in a vacuum dessicator. Matrix (αCyano-4-hydroxycinnamic acid in 50% acetonitrile in sterile water with 0.1% trifluoroacetic acid [TFA]) was applied manually over tissues and peptides and allowed to thoroughly dry before the plate was read in a Voyager DE-Pro Mass Spectrometer (Applied Biosystems, Carlsbad, CA). For tissue lysates, each pituitary was lysed in 100 µL lysis buffer (1 cOmplete™, Mini Protease Inhibitor Cocktail tablet (Roche Life Science, Auckland, New Zealand) dissolved in 10 mL sterile water, 0.1% TFA) on ice using a plastic rod to disrupt tissue followed by sonication in a water bath at 4°C for 2 min. The lysate was then centrifuged at 13,000 rpm at 4C for 2 min. An aliquot (1 µL) of supernatant was mixed with 1 µL of matrix, spotted onto a MALDI-TOF plate, thoroughly dried and then read in a Voyager DE-Pro Mass Spectrometer.

5. Immunoprecipitation and MS to identify the peptide recognized by KM4 antibody in *Pomc*$^{\mathrm{tm1/tm1}}$ mouse pituitary.

KM4 antibody cross-linked to Protein A Sepharose 4 Fast Flow Affinity beads (Roche Diagnostics) was used to pull-down peptides in pituitary lysates. The bound peptides were identified using MALDI-TOF and LC-ESI Mass spectrometry after elution from the beads. The beads were prepared for cross-linking by centrifuging 400 µL Protein A Sepharose 4 bead slurry in an eppendorf tube at 6000rpm for 2 min and removing the ethanol supernatant. The beads were then washed 3 x with 1 mL binding buffer (0.1% BSA in PBS, pH 7.4) by gentle rotation of tubes at room temperature (RT) for 10 min followed by centrifugation and aspiration of supernatant. KM4 antibody (400 µL serum) was bound to the sepharose beads in the presence of 400 µL binding buffer by mixing with rotation overnight at 4°C in the presence of cOmplete™, Mini Protease Inhibitor Cocktail. The beads were then pelleted by centrifugation, the supernatant discarded and the beads were washed once with 400 μL binding buffer followed by 3 washes of 400 μL PBS. The bifunctional coupling reagent, dimethyl pimelindiimidate (DMP) (Sigma-Aldrich New Zealand Ltd, Auckland, NZ) (400 μL), pH 8-9, was added to the beads and they were mixed by rotation for 30 min at RT. Following centrifugation and aspiration of DMP, the beads were washed with 400 μL wash buffer (0.2 M Triethanolamine [Sigma-Aldrich New Zealand Ltd] in PBS) by gentle mixing with rotation for 5 min at RT. The addition of fresh DMP followed by these wash steps was repeated two more times. Quenching buffer (50 mM ethanolamine hydrochloride [Sigma-Aldrich New Zealand Ltd] in PBS, 400 μL) was added to beads followed by gentle mixing by rotation for 5 in at RT, centrifugation and aspiration of supernatant. To remove excess unlabeled antibody, the beads were washed with 0.1 M glycine, pH 3.0. The beads were washed 1x with PBS for 5 min at RT, 3x with PBS + 0.01% sodium azide, 0.1% BSA and then stored in the final wash at 4°C.

Immunoprecipitation using the KM4 cross-linked beads was validated using pure synthetic α-MSH and desacetyl-α-MSH peptides. Sepharose-KM4 cross-linked beads (20 μL slurry) were transferred from the stock into two eppendorf tubes, centrifuged and washed 3x with PBS as previously described. Purified α-MSH (10 μM, 10 μL) or desacetyl-α-MSH (10 μM, 10 μL) was bound to Sepharose-KM4 beads in the presence of 200 μL PBS for 45 min at RT with gentle mixing. Following centrifugation and aspiration of supernatant, the beads were washed 10x with 200 μL wash buffer (50 mM ammonium bicarbonate, pH 8.2) and the final wash was pipetted into a P10 filter tip which when run dry, left the Sepharose-KM4 bead complexed with peptide in the filter. The filter was then washed 10x with 200 μL sterile water before the peptides were eluted into a low-bind eppendorf tube with 10 µL elution buffer (0.1% TFA in acetonitrile). 1 µL of each eluted peptide was spotted onto a MALDI-TOF plate and left to dry in a fume hood overnight. Spots (10 µL) of 2.5 fold dilutions of the 10uM purified peptide stock were included on the plate as positive controls. The following day the spots were analyzed on a Voyager Pro MALDI-TOF Mass Spectrometer as previously described.

Each snap-frozen *Pomc*$^{tm1/tm1}$ mouse pituitary was lysed in 300 µL lysis buffer (50 mM Tris-HCL, 150 mM NaCL, pH 8.0) containing 0.1% Brij 35 (Sigma-Aldrich New Zealand Ltd) + 1 cOmplete™ Mini Protease Inhibitor Cocktail tablet per 10 mL at 4°C using a small plastic homogenizing rod followed by 2 min water bath sonication at 4°C. The homogenate was centrifuged at 13,000 rpm for 2 min at 4°C and the supernatant collected. The supernatant was then incubated with 10 µL Sepharose-KM4 beads at RT for 45 min with gentle mixing. Following centrifugation and aspiration of supernatant the beads were washed as described above for peptide binding and then eluted with 20 µL matrix ready for spotting on MALDI-TOF plate as previously described.

To identify the peptide in *Pomc*$^{tm1/tm1}$ pituitary that immunoprecipitates with KM4, three *Pomc*$^{tm1/tm1}$ pituitaries were immunoprecipitated using KM4 antibody and 1 µL of each eluate was analyzed by MALDI-TOF to confirm the presence of a peak at m/z 4598. The peptide eluates were pooled, diluted 10x in 0.1% formic acid in water and then loaded onto an Oasis Mixed mode Cation Exchange (MCX) SPE cartridge (Waters, Milford, MA, USA). The loaded MCX cartridge was washed 1x with 1 mL 0.1N HCL followed by 1x with 1 mL methanol and then the peptides were eluted with 1 mL 5% ammonium hydroxide in methanol. The eluant was concentrated to ~10-20 µL using centrifugation under vacuum, and then digested with 25 ng/mL sequencinggrade trypsin (Promega, Madison, WI, USA). The resulting digest was separated on a 0.3 x 100 mm Zorbax 300SB-C18 column (Agilent, Santa Clara, CA, USA). The HPLC gradient between Buffer A (0.1% formic acid in water) and Buffer B (0.1% formic acid in acetonitrile) was formed at 6 μL/min as follows: 10% B for the first 3 min, increasing to 35% B by 33 min, increasing to 95% B by 36 min, held at 95% until 39 min, back to 10% B at 40.5 min and held there until 48 min. The LC effluent was directed into the Ionspray source of QSTAR XL hybrid Quadrupole-Time-of-Flight MS (Applied Biosystems, Foster City, CA, USA) scanning from 300-1600 m/z. the top three most abundant multiply-charged peptides were selected for MS/MS analysis (100-1600 m/z). The MS and HPLC system were under the control of the Analyst QS 2.0 software package (Applied Biosystems). The resulting MS/MS spectra were searched against the Mouse subset of NCBI's protein database (146781 sequences, June 2012) using Mascot software (Matrix Science, London, UK).

6. Testing acetyl-QKQR mutant $ACTH_{1\text{-}39}$ peptides for coupling of MC2R and MC4R to adenylyl cyclase *in vitro*.

HEK293 cells stably expressing mouse MC4R (mMC4R) developed previously [4, 5] were used to compare acetyl-QKQR mutant $ACTH_{1\text{-}39}$ with $ACTH_{1\text{-}24}$, $ACTH_{1\text{-}39}$ and QKQR mutant $ACTH_{1\text{-}39}$ to determine whether acetylation of QKQR mutant $ACTH_{1\text{-}39}$ alters QKQR mutant $ACTH_{1\text{-}39}$ activation of the MC4R.

HEK293 cells stably expressing mMRAP developed previously [6] and transiently transfected with mMC2R were used to compare acetyl-QKQR $ACTH_{1\text{-}39}$ with $ACTH_{1\text{-}24}$, $ACTH_{1\text{-}39}$ and QKQR mutant $ACTH_{1\text{-}39}$ to determine whether acetylation of QKQR mutant $ACTH_{1\text{-}39}$ alters mutant QKQR $ACTH_{1\text{-}39}$ activation of the MC2R. The mMC2R was obtained by PCR from *C57BL/6J* mouse retroperitoneal fat cDNA and subcloned into pcDNA3.1 vector (InVitrogen New Zealand Ltd., Auckland, NZ). PCR for mMC2R was performed on 2 μL cDNA using iProof High Fidelity DNA polymerase (BioRad Laboratories Pty, Auckland, NZ) using forward (5'-atcggatccGTAAGTCAACGGCAAACACCACC-3') and reverse (5'-gactcgagCTAATACCGGTTGCAGAAGAGCA-3') and the following conditions: denature at 98°C for 1 min followed by 34 cycles of denature at 98°C, anneal at 62.5°C for 5 s and elongate at 72°C for 10 s, and a final 7 min extension at 72°C. The primers encoded restriction enzyme sites for BamH1 and Xho1 for directional cloning. The recombinant DNA was verified by sequencing and the mMC2R coding sequence aligned with GenBank accession number XM 006525713.1. Adenylyl cyclase activity was determined directly by measuring the ability of cells to convert [^{3}H]adenine to [^{3}H]cAMP following exposure of the cells to increasing doses of peptide as described previously [5].

7. MALDI-TOF Imaging MS.

Pomc$^{wt/wt}$ and *Pomc*$^{tm1/tm1}$ pituitaries from adult mice were dissected, snap frozen and stored at -80°C. Pituitary glands were mounted on a cryostat specimen holder with a small amount of Tissue-Tek OCT Compound (Siemens NZ Ltd.) at the base of the tissue only. Transverse sections (12 μm) were cut and collected alternately via thaw-mounting on glass slides (for histological staining) or stainless steel MALDI plate (for MALDI image analysis). For histological analysis, sections on glass slides were H&E stained using standard procedures. Sections for MALDI imaging analysis were placed in a vacuum desiccator for 30 min prior to undergoing matrix application. A thin even coating of 2,5-dihydroxybenzoic acid (DHB) matrix was applied to pituitary sections using vacuum sublimation. Briefly, the MALDI plate was placed in an in-house fabricated glass sublimation apparatus and a vacuum of 4.0 x 10^{-2} Torr established. Heat (~ 120°C) was applied to the chamber via a sand bath for 6 min to achieve an optimal DHB matrix coating. Following matrix application, matrix was recrystalized using a simple humidity chamber. The MALDI plate was attached to the lid of a glass petri dish and the chamber was closed and humidified with a piece of filter paper saturated with 1 mL of 83.7% acetonitrile and 5% trifluoroacetic acid for 4 min at room temperature. The chamber was then opened and the pituitary sample dried at room temperature.

MALDI imaging was performed using a Voyager DE-Pro MALDI-TOF MS operating in linear positive mode with an accelerating potential of +25 kV. An external calibration was applied to the instrument prior to analysis. MALDI imaging data sets were collected over whole mouse pituitary gland sections (MMSIT, Novartis, Basel Switzerland) with a raster step size of 60 µm and 25 laser shots per spectrum. Each data set consisted of ~1000 individual sampling locations, each representing one pixel in the resultant image. Data were normalized to total ion current and molecular images reconstituted using BioMap software (Novartis, Basel, Switzerland). Each m/z signal was plotted ± 0.05% of the molecular mass. For display purposes, the data were interpolated and pixel intensities were normalized to the maximum intensity for each m/z displayed in the software to use the entire dynamic range. Assignments of peptide identifications were made using tandem MS (data not shown).

8. Plasma corticosterone assay.

Blood was collected from cardiac puncture on isoflurane-anesthetized mice or mice euthanized by cervical dislocation for the dexamethasone suppression tests. Plasma corticosterone was either measured using a commercial kit (Immunodiagnostics, Tyne and Wear, UK) according to the manufacturer's instructions or using triple quadrupole MS. For triple quadrupole MS, 100 µL of internal standard solution (6 ng mL^{-1} corticosterone-d8 in water) was added to 85 µL plasma. Steroids were extracted using 1 mL of ethyl acetate (Merck, KGaA Darnstadt, Germany). After removal of the organic supernatant, samples were dried by vacuum concentration (Savant SC250EXP, Thermo Scientific, Asheville, NC, USA), resuspended in 60 µL of mobile phase (65% methanol (Merck) and 35% water), and transferred to HPLC injector vials. 12 µL was injected onto an HPLC MS system consisting of an Accela MS pump and autosampler followed by an Ion Max APCI source on a Finnigan TSQ Quantum Ultra AM triple quadrapole MS, all controlled by Finnigan Xcalibur software (Thermo Electron Corporation, San Jose, CA, USA). The mobile phase was a gradient of methanol and water, flowing at 300 $\mu L.min^{-1}$ through a Luna HST 2.6µm C18(2) 100 x 3.0mm column at 40ºC (Phenomenex, Auckland, New Zealand). Retention times were 4.3min for both corticosterone and corticosterone-d8. Ionisation was in positive mode for corticosterone and Q2 had 1.2 mTorr of argon. The mass transitions followed were corticosterone 347.15 → 121.1 at 27 V and corticosterone-d8 355.2 → 125.2 at 24 V. All samples were analysed in one assay.

SUPPLEMENTARY REFERENCES

[1] Mitchell, A.R., Kent, S.B.H., Engelhard, M., Merrifield, R.B., 1978. New synthetic route to Tert-Butyloxycarbonylaminoacyl-4-(Oxymethyl)Phenylacetamidomethyl-Resin, an improved support for solid-phase peptide -synthesis. J. Org. Chem. 43: 2845-2852.

[2] Harris, P.W.R., Yang, S.H., Brimble, M.A., 2011. An improved procedure for the preparation of aminomethyl polstyrene resin and its use in solid phase (peptide) synthesis. Tetrahedron Lett. 52: 6024-6026.

[3] Farooqi, I.S., Yeo, G.S., Keogh, J.M., Aminian, S., Jebb, S.A., Butler, G., et al., 2000. Dominant and recessive inheritance of morbid obesity associated with melanocortin 4 receptor deficiency. J. Clin. Invest. 106: 271-279.

[4] Mountjoy, K.G., Kong, P.L., Taylor, J.A., Willard, D.H., Wilkison, W.O., 2001. Melanocortin receptor-mediated mobilization of intracellular free calcium in HEK293 cells. Physiol. Genomics 5: 11-19.

[5] Mountjoy, K.G., Willard, D.H., Wilkison, W.O., 1999. Agouti antagonism of melanocortin-4 receptor: greater effect with desacetyl-alpha-melanocyte-stimulating hormone (MSH) than with alpha-MSH. Endocrinology 140: 2167-2172.

[6] Kay, E.I., Botha, R., Montgomery, J.M., Mountjoy, K.G., 2013. hMRAPalpha increases alphaMSH induced hMC1R and hMC3R functional coupling and hMC4R constitutive activity. J. Mol. Endocrinol. 50: 203-215.

SUPPLEMENTARY FIGURES

Supplementary Figure 1.

Validation that QKQR mutant ACTH functions similar to native $ACTH_{1-39}$. (A) ACTH-stimulated plasma corticosterone in dexamethasone-suppressed adult male mice. Two-hours post dexamethasone treatment mice (n=4 /group) were treated with vehicle (Sham), native $ACTH_{1-39}$ (KKRR) or mutant (QKQR, KGGR, KQRQ)

$ACTH_{1\text{-}39}$ peptide. Data is shown as mean ± SEM ****, $p < 0.0001$. **(B)** Native $ACTH_{1\text{-}39}$, mutant (QKQR) $ACTH_{1\text{-}39}$ and α-MSH stimulated human MC4R co-transfected with Cre-luciferase reporter into HEK293 cells. Data is shown as mean ± SEM for 2-3 independent experiments. **(C)** Plasma corticosterone levels for male (168-216 days) and female (170-208 days) mice. Data are shown as mean ± SEM.

Supplementary Figure 2.

MALDI-TOF MS detects diacetyl-α-MSH and α-MSH in *Pomc*$^{wt/wt}$ but not in *Pomc*$^{tm1/tm1}$ whole pituitary lysates. Mass spectra are shown for representative *Pomc*$^{wt/wt}$ **(A)** and *Pomc*$^{tm1/tm1}$ **(B)** whole pituitary lysates. α-MSH (m/z 1664), diacetyl-α-MSH (m/z 1707) and Arg-CLIP (1-21) (m/z 2359) are detected in *Pomc*$^{wt/wt}$ but not in *Pomc*$^{tm1/tm1}$ pituitary lysates. Vasopressin (m/z 1085), J peptide (m/z 1941) and a peptide that may be β-lipotropin (m/z 4438; 9Da larger than β-lipotropin), are detected in both *Pomc*$^{wt/wt}$ and *Pomc*$^{tm1/tm1}$ pituitary lysates. Relatively weak signal is observed at m/z 4638 for *Pomc*$^{tm1/tm1}$ but not *Pomc*$^{wt/wt}$ pituitary lysates.

Supplementary Figure 3.

N-terminal acetylation does not alter QKQR mutant $ACTH_{1\text{-}39}$ at the mMC4R but it abolishes its activity at the mMC2R. (A) Acetyl-QKQR $ACTH_{1\text{-}39}$ and QKQR $ACTH_{1\text{-}39}$ function identically coupling the mMC4R transfected into HEK293 cells to adenylyl cyclase. Both QKQR mutant $ACTH_{1\text{-}39}$ ($EC_{50} = 4.95 \pm 0.05 \times 10^{-9}$M) and acetyl-QKQR mutant $ACTH_{1\text{-}39}$ ($EC_{50} = 4.74 \pm 0.05 \times 10^{-9}$M) are two-fold less potent compared with native $ACTH_{1\text{-}39}$ ($EC_{50} = 2.23 \pm 0.06 \times 10^{-9}$M). **(B)** QKQR

$ACTH_{1-39}$ is a full agonist coupling the mMC2R transfected into HEK293 cells to adenylyl cyclase but it is 82 fold less potent compared with $ACTH_{1-39}$. In contrast, Acetyl-QKQR ACTH $_{1-39}$ is inactive coupling the mMC2R to adenylyl cyclase. Data is shown as mean ± SEM for three independent experiments.

Supplementary Figure 4.

α-MSH and desacetyl-α-MSH are stable dissolved in PBS when stored at 37 °C for 14 days. MALDI-TOF MS detects (A, C, E) intact α-MSH and (B, D, F) intact desacetyl-α-MSH following (A, B) 7, (C, D) 10 and (E, F) 14 days storage in PBS and incubation at 37 °C. There is no detectable degradation or oxidation of either peptide after 14 days storage. The small peaks observed on MS are likely due to the PBS used to dissolve the peptides.

Figure 1

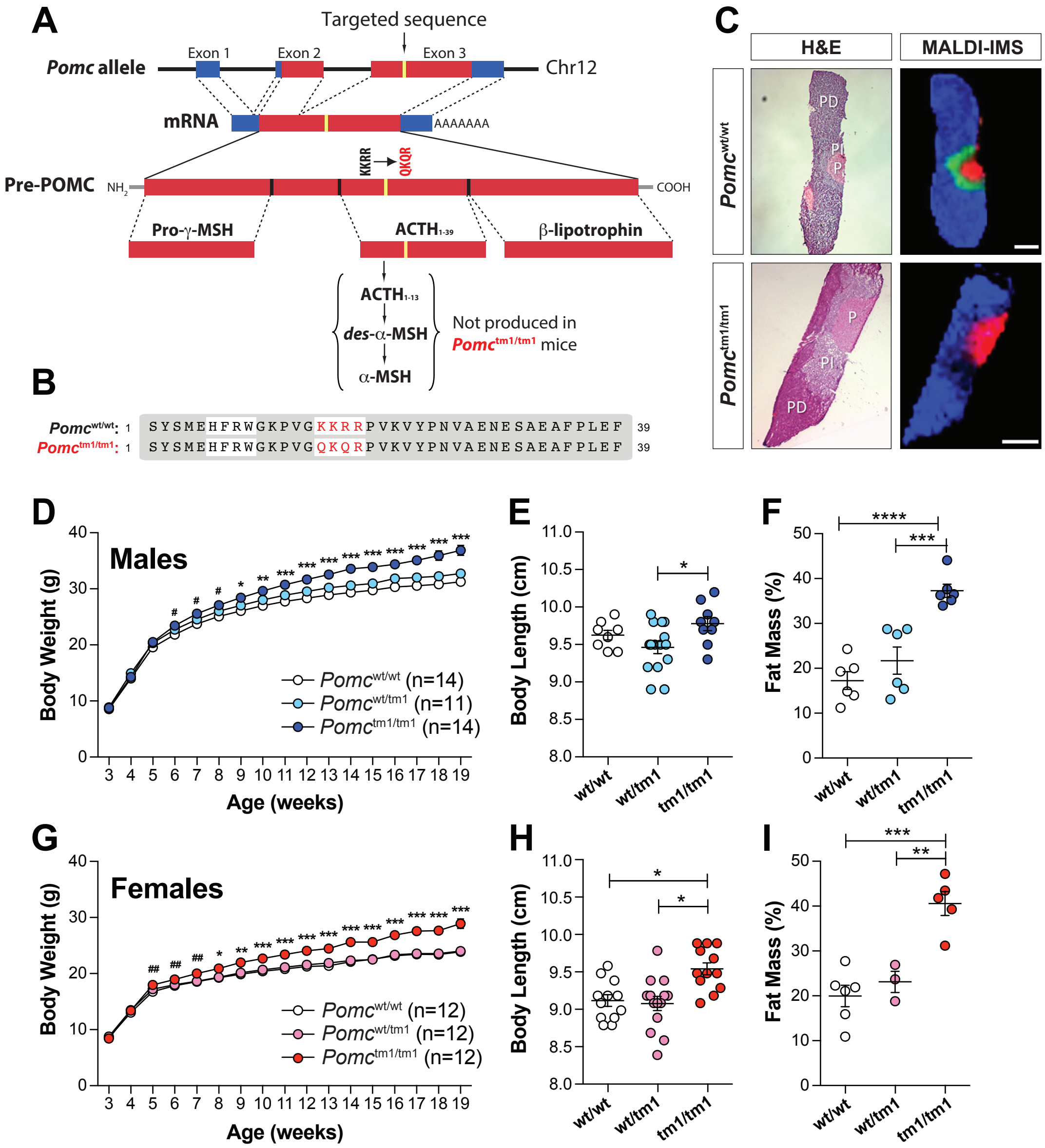

A
Targeted sequence
Pomc allele
Exon 1
Exon 2
Exon 3
Chr12
mRNA
AAAAAAA
Pre-POMC
KKRR
QKQR
COOH
Pro-γ-MSH
ACTH1-39
β-lipotrophin
ACTH1-13
des-α-MSH
α-MSH
Not produced in Pomctm1/tm1 mice
B
Pomcwt/wt: 1 SYSMEHFRWGKPVGKKRRPVKVYPNVAENESAEAFPLEF 39
Pomctm1/tm1: 1 SYSMEHFRWGKPVGQKQRPVKVYPNVAENESAEAFPLEF 39
C
H&E
MALDI-IMS
Pomcwt/wt
Pomctm1/tm1
PD
PI
P
D
Males
Body Weight (g)
Age (weeks)
Pomcwt/wt (n=14)
Pomcwt/tm1 (n=11)
Pomctm1/tm1 (n=14)
E
Body Length (cm)
wt/wt
wt/tm1
tm1/tm1
F
Fat Mass (%)
G
Females
Pomcwt/wt (n=12)
Pomcwt/tm1 (n=12)
Pomctm1/tm1 (n=12)
H
I

Figure 2

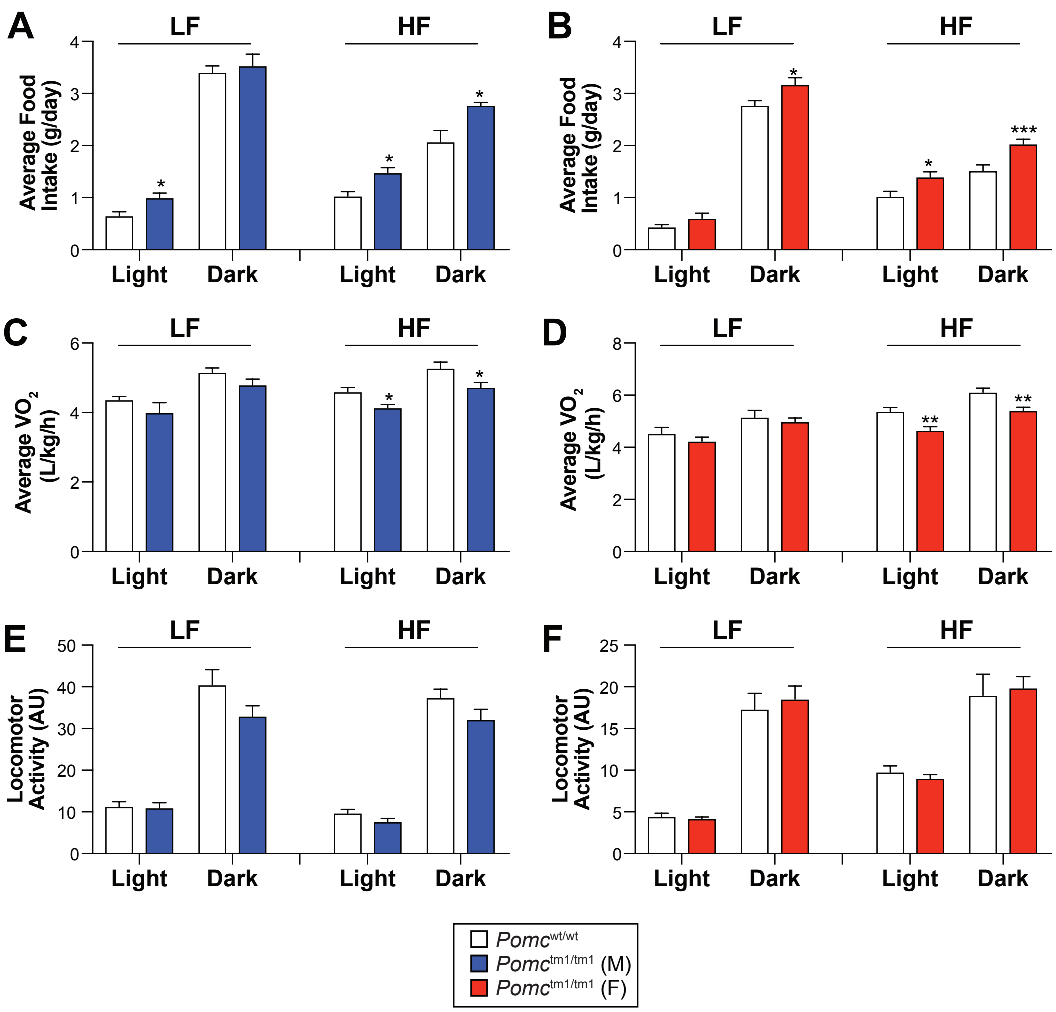

A
B
C
D
E
F
LF
HF
Average Food Intake (g/day)
Average VO2 (L/kg/h)
Locomotor Activity (AU)
Light
Dark
Pomc wt/wt
Pomc tm1/tm1 (M)
Pomc tm1/tm1 (F)

Figure 3

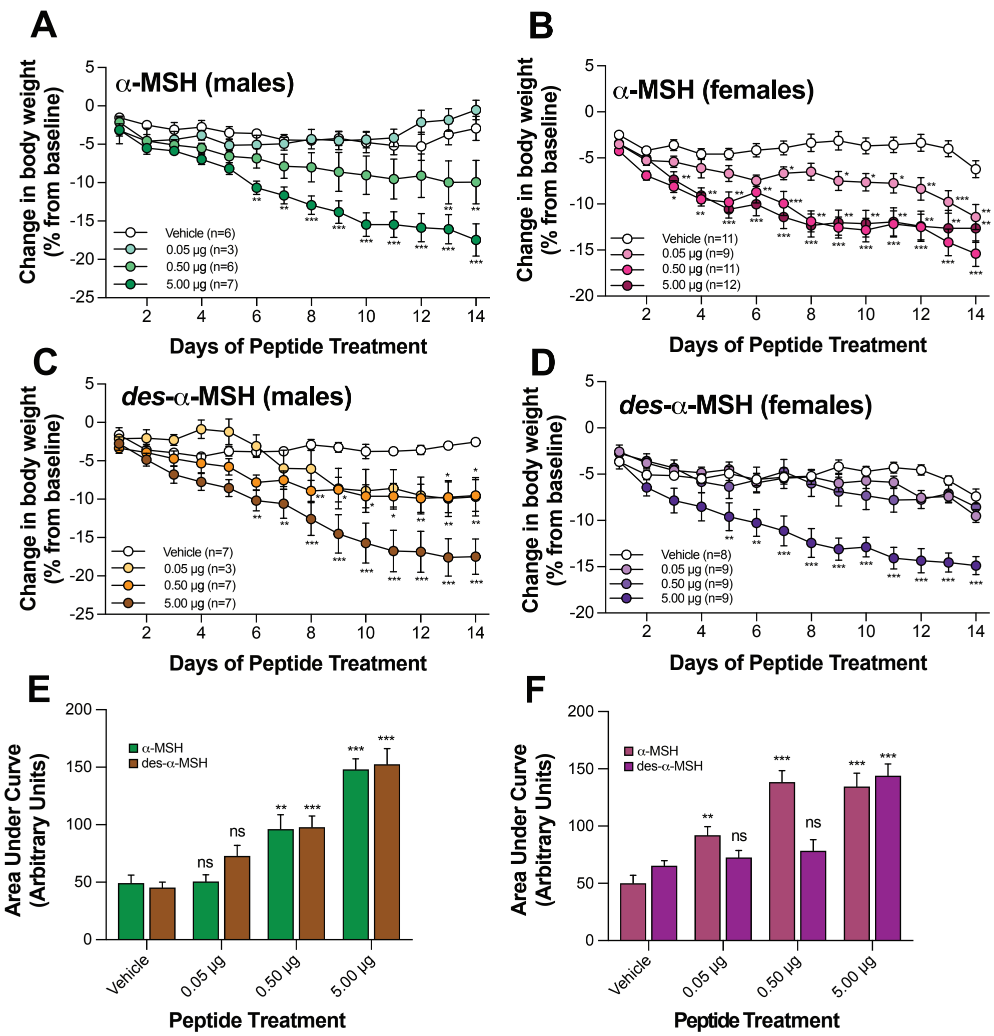
A
α-MSH (males)
Change in body weight (% from baseline)
Vehicle (n=6)
0.05 µg (n=3)
0.50 µg (n=6)
5.00 µg (n=7)
Days of Peptide Treatment
B
α-MSH (females)
Change in body weight (% from baseline)
Vehicle (n=11)
0.05 µg (n=9)
0.50 µg (n=11)
5.00 µg (n=12)
Days of Peptide Treatment
C
des-α-MSH (males)
Change in body weight (% from baseline)
Vehicle (n=7)
0.05 µg (n=3)
0.50 µg (n=7)
5.00 µg (n=7)
Days of Peptide Treatment
D
des-α-MSH (females)
Change in body weight (% from baseline)
Vehicle (n=8)
0.05 µg (n=9)
0.50 µg (n=9)
5.00 µg (n=9)
Days of Peptide Treatment
E
Area Under Curve (Arbitrary Units)
α-MSH
des-α-MSH
Vehicle
0.05 µg
0.50 µg
5.00 µg
Peptide Treatment
F
Area Under Curve (Arbitrary Units)
α-MSH
des-α-MSH
Vehicle
0.05 µg
0.50 µg
5.00 µg
Peptide Treatment

Figure 4

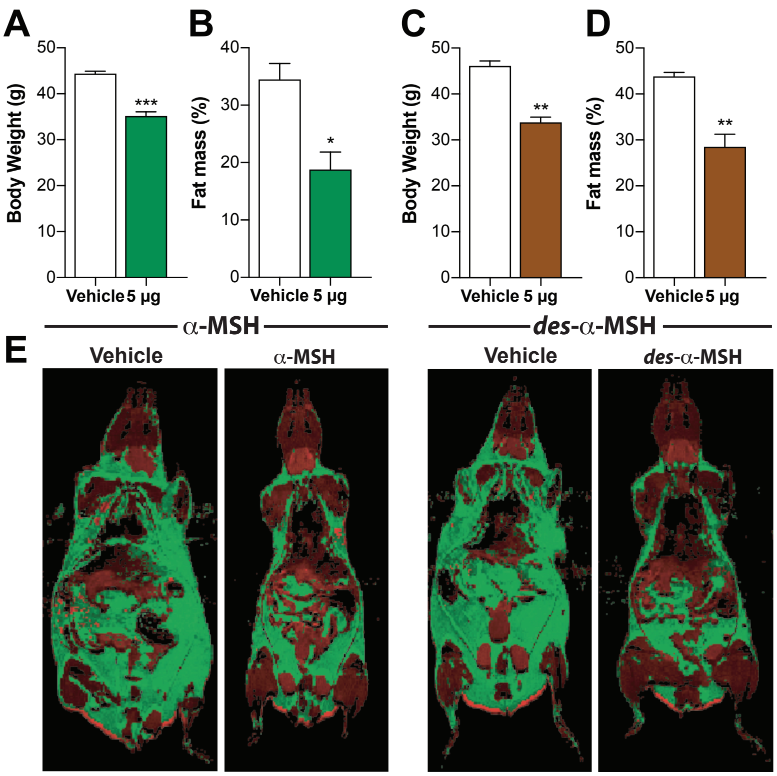

A
B
C
D
Body Weight (g)
Fat mass (%)
50
40
30
20
10
0
***
*
**
**
Vehicle
5 µg
α-MSH
des-α-MSH
E
Vehicle
α-MSH
Vehicle
des-α-MSH

Figure S1

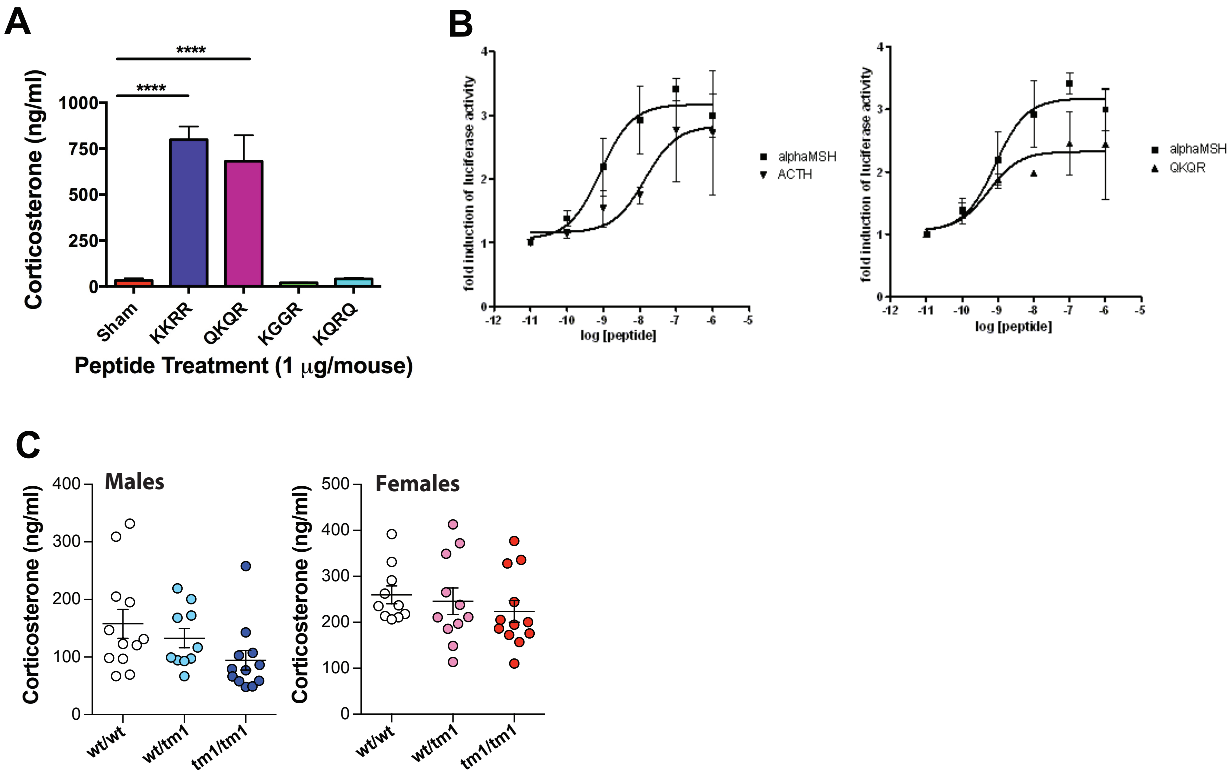
A
****
****
Corticosterone (ng/ml)
1000
750
500
250
0
Sham
KKRR
QKQR
KGGR
KQRQ
Peptide Treatment (1 μg/mouse)
B
fold induction of luciferase activity
log [peptide]
alphaMSH
ACTH
alphaMSH
QKQR
C
Males
Females
Corticosterone (ng/ml)
wt/wt
wt/tm1
tm1/tm1

Figure S2

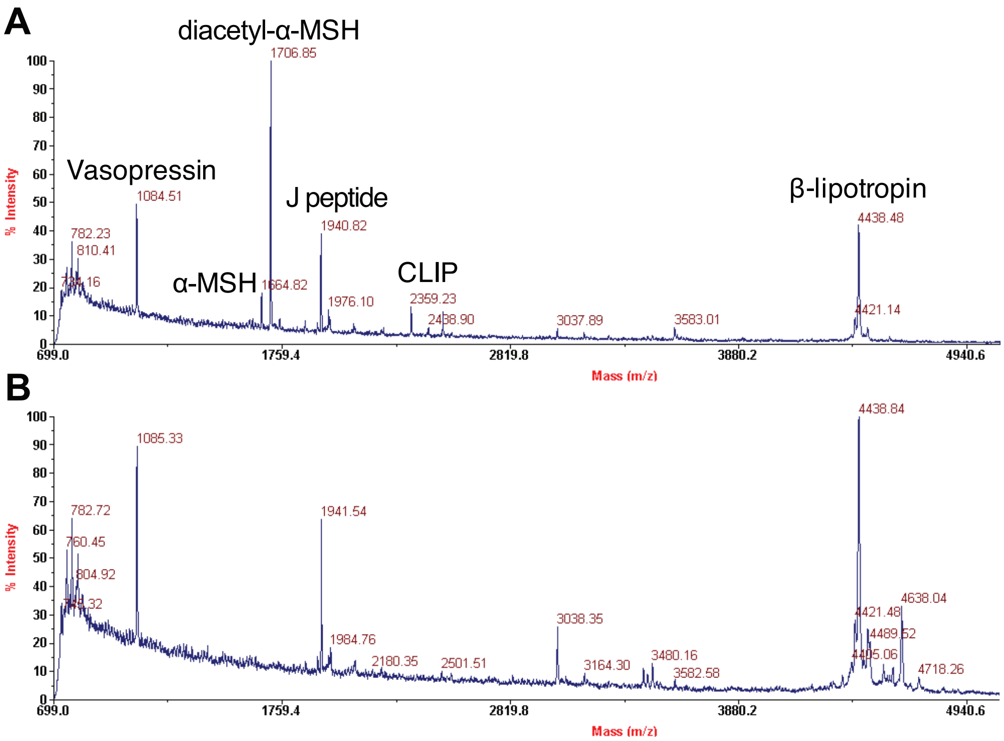

A
diacetyl-α-MSH
1706.85
Vasopressin
1084.51
782.23
810.41
α-MSH
1664.82
J peptide
1940.82
1976.10
CLIP
2359.23
3037.89
3583.01
β-lipotropin
4438.48
4421.14
% Intensity
Mass (m/z)
699.0
1759.4
2819.8
3880.2
4940.6
B
1085.33
782.72
760.45
804.92
1941.54
1984.76
2180.35
2501.51
3038.35
3164.30
3480.16
3582.58
4438.84
4421.48
4638.04
4718.26
% Intensity
Mass (m/z)
699.0
1759.4
2819.8
3880.2
4940.6

Figure S3

A

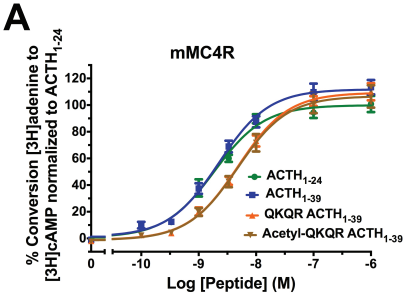

mMC4R
% Conversion [3H]adenine to [3H]cAMP normalized to ACTH1-24
120
100
80
60
40
20
0
ACTH1-24
ACTH1-39
QKQR ACTH1-39
Acetyl-QKQR ACTH1-39
0
-10
-9
-8
-7
-6
Log [Peptide] (M)

B

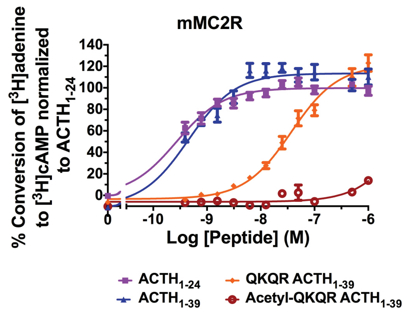

mMC2R
% Conversion of [3H]adenine to [3H]cAMP normalized to ACTH1-24
140
120
100
80
60
40
20
0
0
-10
-9
-8
-7
-6
Log [Peptide] (M)
ACTH1-24
ACTH1-39
QKQR ACTH1-39
Acetyl-QKQR ACTH1-39

Figure S4

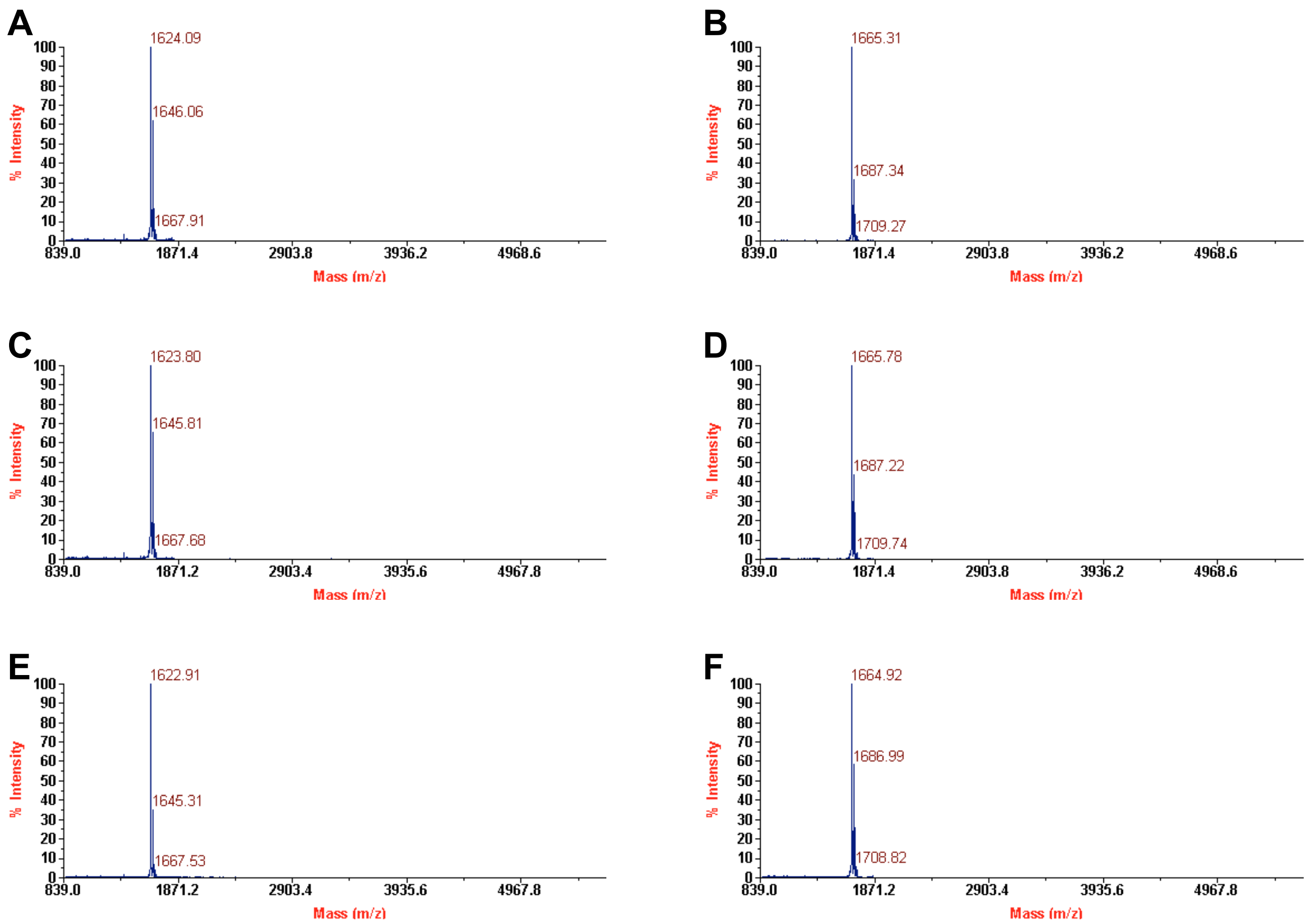
A
1624.09
1646.06
1667.91
B
1665.31
1687.34
1709.27
C
1623.80
1645.81
1667.68
D
1665.78
1687.22
1709.74
E
1622.91
1645.31
1667.53
F
1664.92
1686.99
1708.82
% Intensity
Mass (m/z)
839.0
1871.4
2903.8
3936.2
4968.6
1871.2
2903.4
3935.6
4967.8